

1 Dear Prof. Dr. Claussen, dear reviewers,

2 Thank you very much for your assessment and the constructive comments to improve our
3 manuscript. Our response is detailed below, as well as being reflected in the revised manuscript. We
4 hope that we have addressed all concerns and questions that were raised.

5 With best regards,

6 Minchao Wu (on behalf of all authors)

7

8 **Comments from reviewer #1:**

9

10 (1) Re: Response to (1)

11 In the Rowell (2013) paper, I did not find an evaluation of CanESM2 SSTs – this paper is focused only
12 on the ability of the coupled GCMs to capture the relationship between SSTs and Sahel rainfall (JJAS).
13 According to Fig. 5 in that paper, CanESM2 has particularly weak teleconnections between Sahel
14 rainfall and SSTs, with the exception of the Mediterranean, but I did not find an evaluation of the SST
15 simulation. The Xu paper is only on the southeast tropical Atlantic, and they do not call out the Can
16 ESM2 as being particularly accurate. I really recommend that the authors address this important
17 issue, and consider the possible role of SST biases in precipitation biases.

18 Response: Thanks for suggesting this. We have added an additional figure (Fig. A1 in the revised
19 manuscript), comparing CanESM2 SST and observation-based dataset (HadISST1.1). Given the
20 imperfect simulated SSTs by CanESM2, we agree that its influences on our study should be
21 considered. We revised the discussion from line 263 as:

22 “The SST forcing is important for African climate. SSTs used in the study domain present warm biases
23 up to 5°C for the southeast and equatorial tropical Atlantic, and cold biases for the northern and
24 southern sub-tropic Atlantic and the Mediterranean sea (3rd row, Fig. A1). Such warm biases in the
25 tropical Atlantic, especially in JJA, may partly contribute to the overestimated rainfall in Guinea
26 Coast (Fig. 1b3), and the cold biases in sub-tropics may link to the underestimated rainfall in the
27 Sahel and southern African when comparing to the ERA-Interim driven simulation (NFB-RP, Fig. 1b3;
28 2nd row, Fig. A1). The analyses by Rowell (2013) for the global tropics and by LaRow et al. (2014) and
29 Xu et al. (2014) for tropical sub-regions suggest that the SST biases in CanESM2 are comparable to
30 other CMIP5 models”.

31 (2)Re Responses to (2), (3) and (4)

32 Thank you for addressing these issues more fully.

33 [Response: You are welcome.](#)

34

35 (3)Re Response to (5)

36 I appreciate the rewording. It doesn't help too much in making people understand that the so-called
37 "Charney hypothesis" is incorrect, but it's at least more accurate.

38 [Response: Thanks.](#)

39

40

41 (4)Response to (6)

42 I didn't understand your response – especially the second sentence was not clear. Are you saying the
43 20 c. vegetation forcing is too small to have an effect? Or the difference in averaging periods is
44 important? What about the 21 st c. conditions will make vegetation forcing more prominent?

45 [Response: We wanted to state that the contrasting influences from the static \(RCA\) and dynamic
46 \(RCA-GUESS\) vegetation is very limited in the 20th century. When climate starts to change, the
47 impact of dynamic vegetation becomes visible between prescribed \(present-day\) vegetation and
48 dynamically changing vegetation. Hence, the comparison of present-day precipitation with a
49 previous version of RCA does not show any evaluation of the importance of vegetation dynamics,
50 but only confirms the new version of RCA to result in similar precipitation.](#)

51

52 (5)I stand corrected on the savanna/savannah spelling!

53 [Response: Thanks.](#)

54

55

56

57

58

59

60

61

62

63 **Comments from reviewer #2:**

64 The authors have addressed most of my previous comments.

65 I do have two additional comments that are minor but important in improving the quality of the
66 paper:

67 1) This is of course not the first study of this type conducted for this region. It is important that
68 results be compared with those of previous studies, at least qualitatively. Any similarity? Any major
69 differences? This discussion (preferably in the last section of the paper) is important for guiding
70 future studies.

71 Response: Thanks for suggesting this, some statements to compare previous similar study have
72 been added in the discussion section 4.3, as:

73 “Similar to the local effects over semiarid region identified in a previous vegetation-feedback study
74 focusing on an African sub-domain (Yu et al., 2015), in which vegetation feedback increases local
75 precipitation, our study in advance presents a remote effect induced by vegetation feedback over
76 the African wet tropics that may not be easy to capture in a smaller simulation domain. A larger
77 domain including sufficient adjacent ocean could enhance land-ocean interaction through changes in
78 regional circulation and allow regional teleconnection features, e.g. the influences of the tropical
79 Atlantic on rainfall in Guinea Coast and central Africa (Camberlin et al., 2001; Nicholson and Grist,
80 2003), and link between the Mediterranean Sea and Sahelian rainfall (Rayner et al., 2003), to
81 develop”

82

83 2) In addressing one of my previous comments about severe model biases, the authors added a
84 paragraph where the biases in the model was referred to "initial state". This is extremely misleading.
85 It leaves the wrong impression that the bias might be just within the model initial conditions, which
86 is not true. The biases shown are biases related to model structure that will stay with the model
87 throughout the whole simulation. Please correct this misuse of terminology.

88 Response: Thanks for spotting this out. Some words in the last paragraph in section 4.2 are
89 misleading indeed. We have corrected the statement as:

90 Line 483: “... climate forcing, are large relative to the bias ...” → “... climate forcing, are large
91 compared to the bias ...”

92 Line 527: “Despite biases in the present-day precipitation” → “Despite biases in the initial
93 precipitation”

94

95

96

97

98

99 **Reference:**

100 Camberlin, P., Janicot, S., and Pocard, I.: Seasonality and atmospheric
101 dynamics of the teleconnection between African rainfall and tropical sea -
102 surface temperature: Atlantic vs. ENSO, *International Journal of*
103 *Climatology*, 21, 973-1005, 2001.

104 LaRow, T. E., Stefanova, L., and Seitz, C.: Dynamical simulations of north
105 Atlantic tropical cyclone activity using observed low-frequency SST
106 oscillation imposed on CMIP5 Model RCP4.5 SST projections, *Journal of*
107 *Climate*, 27, 8055-8069, 2014.

108 Nicholson, S. E., and Grist, J. P.: The seasonal evolution of the
109 atmospheric circulation over West Africa and equatorial Africa, *Journal of*
110 *Climate*, 16, 1013-1030, 2003.

111 Rayner, N., Parker, D. E., Horton, E., Folland, C., Alexander, L., Rowell, D.,
112 Kent, E., and Kaplan, A.: Global analyses of sea surface temperature, sea ice,
113 and night marine air temperature since the late nineteenth century, *Journal*
114 *of Geophysical Research: Atmospheres*, 108, 2003.

115 Rowell, D. P.: Simulating SST teleconnections to Africa: What is the state
116 of the art?, *Journal of Climate*, 26, 5397-5418, 2013.

117 Xu, Z., Chang, P., Richter, I., and Tang, G.: Diagnosing southeast tropical
118 Atlantic SST and ocean circulation biases in the CMIP5 ensemble, *Climate*
119 *dynamics*, 43, 3123-3145, 2014.

120 Yu, M., Wang, G., and Pal, J. S.: Effects of vegetation feedback on future
121 climate change over West Africa, *Climate Dynamics*, 1-20, 2015.

122

123

124

125

126 **Vegetation-climate feedbacks modulate rainfall patterns in Africa under**
127 **future climate change**

128 M. Wu¹, G. Schurgers², M. Rummukainen^{1,3}, B. Smith¹, P. Samuelsson⁴, C. Jansson⁴, J.
129 Siltberg¹, W. May^{3,5}

130 [1]{Department of Physical Geography and Ecosystem Science, Lund University, Sölvegatan 12, SE-
131 223 62, Lund, Sweden}

132 [2]{Department of Geosciences and Natural Resource Management, University of Copenhagen,
133 Øster Voldgade 10, DK-1350 Copenhagen, Denmark}

134 [3]{Centre for Environmental and Climate Research, Lund University, Sölvegatan 37, SE-223 62 Lund,
135 Sweden}

136 [4]{Rosby Centre, Swedish Meteorological and Hydrological Institute, SE-601 76, Norrköping,
137 Sweden}

138 [5]{Research and Development Department, Danish Meteorological Institute, Lyngbyvej 100, DK-
139 2100 Copenhagen, Denmark}

140

141

142 Correspondence to: M. Wu (minchao.wu@nateko.lu.se)

143

144

145

146

147

148

149

150

151

152

153

154

155 ***Abstract***

156 Africa has been undergoing significant changes in climate and vegetation in recent decades,
157 and continued changes may be expected over this century. Vegetation cover and
158 composition impose important influences on the regional climate in Africa. Climate-driven
159 changes in vegetation structure and the distribution of forests versus savannah and
160 grassland may feed back to climate via shifts in the surface energy balance, hydrological
161 cycle and resultant effects on surface pressure and larger-scale atmospheric circulation. We
162 used a regional Earth system model incorporating interactive vegetation-atmosphere
163 coupling to investigate the potential role of vegetation-mediated biophysical feedbacks on
164 climate dynamics in Africa in an RCP8.5-based future climate scenario. The model was
165 applied at high resolution (0.44 x 0.44 degrees) for the CORDEX-Africa domain with
166 boundary conditions from the CanESM2 GCM. We found that increased tree cover and leaf-
167 area index (LAI) associated with a CO₂ and climate-driven increase in net primary
168 productivity, particularly over sub-tropical savannah areas, not only imposed important local
169 effect on the regional climate by altering surface energy fluxes, but also resulted in remote
170 effects over central Africa by modulating the land-ocean temperature contrast, Atlantic
171 Walker circulation and moisture inflow feeding the central African tropical rainforest region
172 with precipitation. The vegetation-mediated feedbacks were in general negative with
173 respect to temperature, dampening the warming trend simulated in the absence of
174 feedbacks, and positive with respect to precipitation, enhancing rainfall reduction over the
175 rainforest areas. Our results highlight the importance of accounting for vegetation-
176 atmosphere interactions in climate projections for tropical and sub-tropical Africa.

177

178 **Keywords:** RCA-GUESS, Vegetation Dynamics, Biophysical feedback, Precipitation,
179 Walker Circulation, Land-ocean Contrast, Regional Climate Model

180

181

182

183

184

185

186

187

188

189

190

191

192

193

194

195

196

197

198

199

200

201

202

203

204 ***1. Introduction***

205 The Sahel greening and Congo rainforest browning observed since the 1980s suggest that
206 Africa has been undergoing significant changes in the structure, composition and
207 distribution of vegetation during recent decades (Eklundh and Olsson, 2003;Olsson et al.,
208 2005;Jamali et al., 2014;Zhou et al., 2014). In addition to influences from anthropogenic
209 activity (e.g. changes in land use), vegetation changes in the region have been linked to
210 changes in recorded climatic conditions, including the trend and interannual variability of
211 precipitation (Herrmann et al., 2005;Hickler et al., 2005;Olsson et al., 2005;Zhou et al., 2014),
212 which in turn have been related to decadal-scale changes in regional circulation (Camberlin
213 et al., 2001;Giannini et al., 2003). On longer timescales, anthropogenic climate change has
214 the potential to cause profound structural and compositional changes in vegetation over
215 Africa (Sitch et al., 2008;Scheiter and Higgins, 2009).

216 Shifts in vegetation cover and composition in terms of the distribution of trees and
217 grasses and their seasonal changes (phenology) can impose significant forcings on the
218 physical climate system by modulating surface-atmosphere energy exchange and
219 hydrological cycling, resulting in biophysical feedbacks along with the climate forcings. The
220 type of vegetation alongside productivity-related structural aspects such as tree density and
221 leaf area index (LAI) are important determinants for surface albedo, roughness length and
222 evapotranspiration, affecting surface energy fluxes that in turn control lower boundary layer
223 thermodynamics (Eltahir, 1996;Brovkin et al., 2006;Bonan, 2008). Biophysical feedbacks
224 operate locally and may also generate teleconnections via heat and moisture advection,
225 leading to altered atmospheric circulation (e.g. Avissar and Werth, 2005;Nogherotto et al.,
226 2013). Previous studies have shown the importance of vegetation-mediated biophysical

227 feedbacks for the past (e.g. Claussen and Gayler, 1997;Texier et al., 1997), and present (e.g.
228 Eltahir, 1996;Claussen, 1998;Wang and Eltahir, 2000) climate over Africa. Hypothesised
229 mechanisms of vegetation-atmosphere coupling include modulations of the surface albedo
230 (Charney, 1975), changes in the North-African monsoon system (Claussen, 1997) and
231 internal climate variability (Zeng et al., 1999).

232 Feedbacks mediated by shifts in vegetation structure and distribution can likewise play a
233 role for the future regional climate. General circulation models (GCMs) have been applied at
234 relatively coarse lateral grid resolutions to capture these dynamics (e.g. Kucharski et al.,
235 2013). Recent studies have used a regional climate model to investigate the impact of
236 climate-vegetation interaction for West Africa, identifying significant vegetation feedback in
237 modulating local hydrological cycling (e.g. Alo and Wang, 2010;Wang and Alo, 2012;Yu et al.,
238 2015). Additionally, a number of GCM-based studies have investigated the climate effects of
239 anthropogenic perturbations, such as deforestation or afforestation (e.g. Lawrence and
240 Vandecar, 2015). Such studies point to potentially significant forcing of regional climate
241 dynamics, particularly rainfall patterns, as a result of changes in land cover. No study to date
242 has, however, characterised the coupled dynamics of vegetation and climate under future
243 radiative forcing for the entire African domain at a grid resolution high enough to capture
244 regional features and forcings.

245 In this study, we employ a regional Earth system model (ESM) that couples the physical
246 component of a regional climate model (RCM) with a detailed, individual-based dynamic
247 vegetation model (DVM). This tool enables dynamic representation of biophysical
248 interactions between the vegetated land surface and the atmosphere and their effects on
249 the evolution of climate and land surface biophysical properties to be analysed in an explicit

250 way. We perform simulations under the Representative Concentration Pathway (RCP) 8.5
251 radiative forcing scenario (Moss et al., 2010) with and without vegetation feedbacks
252 enabled, and investigate the potential coupled evolution of climate and vegetation for the
253 African continent over the 21st century. Our focus is especially on the central African
254 rainforest areas and the surrounding savannah vegetation belt.

255 ***2. Data and Method***

256 ***2.1 Model description***

257 RCA-GUESS (Smith et al., 2011) is a regional ESM based on the Rossby Centre regional
258 climate model RCA4 (Kjellström et al., 2005;Samuelsson et al., 2011) coupled with
259 vegetation dynamics from the LPJ-GUESS DVM to account for land-atmosphere biophysical
260 coupling (Smith et al., 2001;Smith et al., 2014).

261 The RCA4-based physical component of RCA-GUESS incorporates advanced regional surface
262 heterogeneity, such as complex topography and multi-level representations for forests and
263 lakes, which are significant in controlling the development of weather events from the local-
264 to meso-scale (Samuelsson et al., 2011). RCA4 has been applied in a range of climate
265 studies worldwide (e.g., Döscher et al., 2010;Kjellström et al., 2011;Sörensson and
266 Menéndez, 2011). The land surface scheme (LSS, Samuelsson et al., 2006) adopts a tile
267 approach and characterizes land surface with open land and forest tiles with separate
268 energy balances. The open land tile is divided into fractions for vegetation (herbaceous
269 vegetation) and bare soil. The forest tile is vertically divided into three sub-levels (canopy,
270 forest floor and soil). Surface properties such as surface temperature, humidity and
271 turbulent heat fluxes (latent and sensible heat fluxes) for different tiles in a grid box are

272 weighted together to provide grid-averaged values. A detailed description is given by
273 Samuelsson et al. (2006).

274 The vegetation dynamics component of RCA-GUESS employs a plant individual and patch-
275 based representation of the vegetated landscape, optimized for studies at regional and
276 global scale. Heterogeneities of vegetation structure and their effects on ecosystem
277 functions such as carbon and water vapour exchange with the atmosphere are represented
278 dynamically, affected by allometric growth of age-size classes of woody plant individuals,
279 along with a grass understorey, and their interactions in competition for light and soil
280 resources. Plant functional types (PFTs) encapsulate the differential functional responses of
281 potentially-occurring species in terms of growth form, bioclimatic distribution, phenology,
282 physiology and life-history characteristics. Multiple patches in each vegetated tile account
283 for the effects of stochastic disturbances, establishment and mortality on local stand history
284 (Smith et al., 2001). This explicit, dynamic representation of vertical structure and landscape
285 heterogeneity of vegetation has been shown to result in realistic simulated vegetation
286 dynamics in numerous studies using the offline LPJ-GUESS model (Smith et al., 2001;Weber
287 et al., 2009;Hickler et al., 2012;Smith et al., 2014;Wårlind et al., 2014;Wu et al., 2015).

288 Biophysical feedbacks have previously been studied in applications of RCA-GUESS to Europe
289 and the Arctic (Wramneby et al., 2010;Smith et al., 2011;Zhang et al., 2014). A general
290 description of the coupling between the vegetation dynamics component LPJ-GUESS and
291 the physical component RCA is provided in the Appendix. A more detailed description is
292 given by Smith et al. (2011).

293 **2.2 Model setup, experiments and analysis approach**

294 The simulations were applied over the African domain of the Coordinated Regional Climate
295 Downscaling Experiment (CORDEX-Africa, Giorgi et al., 2009; Jones et al., 2011) on a
296 horizontal grid with a resolution of $0.44^\circ \times 0.44^\circ$. The period studied was 1961 to 2100.
297 Forcing fields in 6-hour time intervals (atmospheric fields and sea-surface temperature (SST)
298 as lateral and lower boundary conditions, respectively) were derived from the historical and
299 RCP8.5 simulations with the CanESM2 general circulation model (GCM) (Arora et al., 2011)
300 in the Coupled Model Intercomparison Project Phase 5 (CMIP5, Taylor et al., 2012). Time-
301 evolving forcing fields from the GCM were prescribed for all variables, including SSTs.

302 The vegetation sub-model LPJ-GUESS was set up with eight PFTs which represent the major
303 elements of natural vegetation across Africa, including the tropical and warm-temperate
304 forests and savannahs and C_3 and C_4 grasslands. The PFT parameter settings follow Morales
305 et al. (2007) and are summarised in Table A1.

306 PFTs of the forest tile were simulated with 30 replicate patches. Average values of state
307 variables across the replicate patches were used to determine biophysical parameters, i.e.
308 forest fraction and LAI for trees versus grasses, provided as forcing to the physical sub-
309 model. For the open land tile with herbaceous species, C_3 and C_4 grass were simulated
310 deterministically and aggregated to characterise open land vegetation. Fire disturbance in
311 response to climate and simulated fuel load (Thonicke et al., 2001) was included.

312 Following the approach of Wramneby et al. (2010) and Smith et al. (2011), RCA-GUESS was
313 initialized with a spin-up in two stages to achieve a quasi-steady state representative for
314 mid-1900's conditions. After the spin-up, the model was run in coupled mode from 1961
315 onwards, with simulated meteorological forcing from the physical sub-model affecting
316 vegetation phenology and structural dynamics, and biophysical land surface properties

317 being adjusted to reflect the changes in vegetation, thereby affecting the physical climate
318 dynamics. For comparison, a recent past experiment (RP, Table 1) with the same vegetation
319 spin-up but thereafter driven by boundary conditions derived from ECMWF re-analysis (ERA-
320 Interim) (Berrisford et al., 2009), was conducted for the period 1979-2011.

321 The simulation protocol was designed to enable biophysical feedbacks of vegetation
322 changes to the evolving 21st century climate to be inferred. Three simulations were
323 performed to investigate vegetation-climate feedbacks under future climate change (Table
324 1). The first simulation included the vegetation feedback (FB). It was run for 1961-2100 in
325 coupled mode, allowing the effects of climate and atmospheric CO₂ concentration (the
326 latter taken directly from the RCP 8.5 data set) on vegetation state to feed back to the
327 evolving climate. The second simulation was run with vegetation feedback “switched off”
328 (non-feedback run, NFB). It started with the state of FB simulation at 1991 and used a
329 prescribed climatology of daily vegetation for 1961-1990 from the coupled simulation, but
330 without transferring the simulated changes in vegetation in LPJ-GUESS to the land surface
331 configuration, and associated biophysical surface properties, in the LSS of RCA. To attribute
332 the component of the simulated vegetation changes resulting from physiological effects of
333 rising CO₂ concentrations of plant productivity and water-use efficiency, we performed a
334 third simulation (FB_CC), which was similar to FB, but started from the state of the FB
335 simulation of 1991 and used historical atmospheric CO₂ concentrations until 2005, held
336 constant thereafter, to force the vegetation sub-model only.

337 Our analysis focuses on the future period 2081-2100, comparing this with the present-day
338 (1991-2010). The climate change signal is inferred from the difference between the future

339 mean and the present-day mean in the NFB run. Vegetation feedbacks are calculated as the
340 difference between the future means of the FB and NFB runs.

341 **2.3 Methods to evaluate model performance**

342 Simulated near-surface atmospheric temperature over open land, precipitation, and LAI
343 were compared against observations within the common available time period 1997-2010.
344 Temperature and precipitation were compared with gridded observations from the CRU
345 TS3.23 (Harris et al., 2014) dataset, focusing on the annual mean and seasonality. For
346 precipitation we also employed the GPCP (Huffman et al., 2001, version 1.2 of One-Degree
347 Daily product for 1996/10-2011/6) which uses satellite data to upscale rain gauge
348 measurements and has been extensively used for African precipitation studies (e.g., Nikulin
349 et al., 2012). For the LAI evaluation we used the GIMMS-AVHRR and MODIS-based LAI3g
350 product (Zhu et al., 2013) which has been previously applied to the evaluation of vegetation
351 dynamics in ESMs (e.g., Anav et al., 2013).

352 To identify biases propagating from the model physics and from the GCM-derived boundary
353 forcing data, we compared the reanalysis-driven RP simulation against observation and
354 against the GCM-driven (CanESM2) FB simulation for the same period.

355 **3. Results**

356 **3.1 Model evaluation**

357 To evaluate the model's performance for the present day, the simulated annual mean and
358 seasonality of 2-meter air temperature, precipitation and LAI are compared against the
359 observations (Fig. 1 and Fig. 2). The simulated annual mean temperature (Fig. 1a1) is
360 generally higher in northern-hemisphere (hereinafter "northern") Africa than in southern-

361 hemisphere (hereinafter “southern”) Africa. The model generally shows a cold bias in the
362 order of 1°C for northern and southern savannah (Fig. 1a2), dominated by the northern
363 hemisphere summer (JJA, Fig. 2a1,2a3). Warm biases up to around 3°C occur in northern
364 Africa, and warm biases up to around 1°C in central Africa where the warm bias originates
365 mainly from summer (Fig. 2a2).

366 The simulated precipitation is largest over western and central Africa up to 1600 mm
367 year⁻¹ within the simulated rainbelt between 25°N and 25°S, where the Atlantic moisture
368 inflow (monsoon and equatorial westerlies) plays an important role (Fig. 1b1). Comparison
369 with CRU reveals a considerable dry bias (-500 mm year⁻¹) for the central African rainforest
370 area and a wet bias (+250 mm year⁻¹) for the northern savannah. The simulated patterns and
371 magnitude of precipitation for this area are similar to a previous study using an earlier
372 version of RCA, RCA3.5, without dynamic vegetation (Nikulin et al., 2012). In RCA, the dry
373 bias for annual mean precipitation over central Africa may be partly due to the
374 underestimated daily precipitation during the late afternoon and night in addition to
375 observational uncertainties (Nikulin et al., 2012). The wet bias over the northern savannah is
376 mainly caused by a too early onset of the rainy season (b1, Fig. 2), which is possibly caused
377 by the interactions between the simulated deep convection and the Africa Easterly Waves
378 (Sylla et al., 2011). The biases in simulated precipitation for the savannah regions and the
379 central African rainforest area mirror the temperature biases: warm biases coincide with dry
380 biases in central Africa, and cold biases coincide with wet biases in savannah regions. A
381 comparison of the CanESM2-driven (FB run) and the ERA-Interim-driven (RP run) simulations
382 (Fig. 1b3) indicates that the bias in simulated precipitation has contributions both from the
383 RCM itself and from the GCM-generated boundary conditions. Nevertheless, Nikulin et al.

384 (2012) have previously shown for Africa that the model is able to capture the ITCZ position
385 and the main features of the seasonal mean rainfall distribution and its annual cycle, and
386 the model biases in precipitation were of similar magnitude to the differences between
387 observational datasets.

388 The SST forcing is important for African climate. SSTs used in the study domain present
389 warm biases up to 5°C for the southeast and equatorial tropical Atlantic, and cold biases for
390 the northern and southern sub-tropic Atlantic and the Mediterranean sea (3rd row, Fig. A1).
391 Such warm biases in the tropical Atlantic, especially in JJA, may partly contribute to the
392 overestimated rainfall in Guinea Coast (Fig. 1b3), and the cold biases in sub-tropics may link
393 to the underestimated rainfall in the Sahel and southern African when comparing to the
394 ERA-Interim driven simulation (NFB-RP, Fig. 1b3; 2nd row, Fig. A1). The analyses by Rowell
395 (2013) for the global tropics and by LaRow et al. (2014) and Xu et al. (2014) for tropical sub-
396 regions suggest that the SST biases in CanESM2 are comparable to other CMIP5 models. To
397 further diagnose the effect of model dynamics on the precipitation bias, we evaluated the
398 low-level circulation and humidity, which play an important role in the moisture transport
399 between ocean and land (Nicholson and Grist, 2003). ~~The SST forcing is also important for~~
400 ~~the African climate, and the CanESM2 SSTs have been validated and shown to be accurate in~~
401 ~~previous studies (e.g. Rowell, 2013; LaRow et al., 2014; Xu et al., 2014).~~ We compare the
402 simulated circulation and specific humidity at 850 hPa from the NFB run with the regional
403 model against ERA-Interim reanalysis for 1997-2010 (Fig. A12). The simulated patterns of
404 circulation and specific humidity at 850 hPa agree well with the reanalysis: the trade winds
405 over both northern and southern Atlantic, West African monsoon as well as the Somali Jet
406 (eastern Africa) are reproduced well by the model. However, there are small biases in wind

407 speed at 850 hPa which generally appear in areas close to the domain boundary and around
408 the African coastal regions. In the case of specific humidity, there are dry biases over the
409 continent. These may be traceable to the different convective schemes used in RCA and
410 ERA-Interim, exhibiting different diurnal cycle of precipitation over Africa (Nikulin et al.,
411 2012).

412 The simulated seasonality of LAI generally reflects the simulated seasonality of precipitation.
413 A systematic overestimation is apparent for savannahs, and a significant underestimation
414 for the central Africa rainforest area. These biases in LAI predominantly reflect the
415 corresponding biases in precipitation (Fig. 2 b1-b3 and 2c1-c3). A stronger LAI bias in the
416 savannah is due to the presence of grasses, which are more sensitive to precipitation
417 changes in the model compared to trees.

418 With present-day forcing, the simulated climate and vegetation patterns and phenology are
419 generally consistent with observations. Some of the biases in the simulated climate are
420 common to many RCMs (Nikulin et al., 2012) and they are apparent for some sub-regions
421 and seasons in our model. We conclude that the performance is adequate to capture the
422 main details of the African climatology, providing sufficient confidence for the subsequent
423 analysis of regional vegetation-climate interactions under future climate change.

424 ***3.2 Future climate and vegetation change***

425 In the NFB simulation, most of the African continent is simulated to be 4-6°C warmer by the
426 end of the 21st century compared with present day (Fig. 3a). The subtropics exhibit a slightly
427 stronger warming than the tropics, and land warming is slightly larger compared to warming
428 of the surrounding ocean surface as simulated by the CanESM2 GCM and represented in the

429 SST forcing fields prescribed from that model. These changes are fairly similar throughout
430 the year, except in Northern Africa and the Sahara, where the temperature increase is
431 particularly pronounced in the local dry season (Fig. [A3.e-h](#)). Precipitation is projected to
432 increase in most parts of the African monsoon area, western equatorial coastal area and the
433 eastern African horn (Fig. [A4.e-h](#)). A slight decrease is projected in the Congo basin and for
434 the southern part of the continent (Fig. 3c). For areas with a precipitation increase, the
435 increase is mainly confined to the local wet season. The precipitation decrease over central
436 and southern Africa is apparent throughout the year (Fig. [A4.e-h](#)).

437 Vegetation feedbacks (FB run) modify significantly the pattern and magnitude of simulated
438 climate change. The effects are largest in low-latitude areas where the surface temperature
439 increase is generally dampened (negative feedback), most notably in savannah areas and to
440 a lesser extent in the equatorial rainforest area (Fig. 3b). The precipitation decrease is
441 enhanced (positive feedback), most notably over the rainforest area (Fig. 3d).

442 With the effects of climate change and CO₂ fertilization, future vegetation growth depicts an
443 enhancement not only of vegetation productivity in general, but also of tree cover in
444 subtropical savannah areas (Fig. 4a), displacing grasses and reflecting an increase in tree LAI
445 of 0.5-2.4 during the growing season (Fig. 4b). This increase in tree cover reflects a general
446 rise in vegetation productivity driven by rising atmospheric CO₂ concentrations on
447 photosynthesis and water-use efficiency (Long, 1991;Hickler et al., 2008;Keenan et al.,
448 2013). Results from the FB_CC experiment in which CO₂ fertilisation was disabled reveal that
449 changes in climate drivers alone are simulated to have minor or opposing effects on tree
450 productivity and LAI due to reduced water availability (Fig. [A5.](#)), and that the changes seen in
451 tree cover and LAI in the FB run hence originate primarily from CO₂ fertilization.

452 Temperature feedbacks tend to be strong in areas of increased tree cover (Fig. 3b, Fig. 4a).
453 The cooling effects from vegetation feedbacks are strong (approximately -2°C) throughout
454 the year, with the most pronounced cooling occurring in the local dry season (Fig. A3.i-l),
455 when the newly established tree (with larger root depth than grass) transpires water that is
456 taken up from the deeper soil layer. Transpiration from present-day grass is constrained by
457 the low moisture levels in the top soil layer. As a result, the evaporative cooling effect
458 becomes stronger when forest replaces open land. In the central African rainforest area,
459 where an increase in LAI of about 0.5-1 is simulated in FB run compared with the NFB run,
460 vegetation feedbacks on temperature are much smaller in the rainy season, but cause
461 cooling in the dry season.

462 Vegetation feedbacks on precipitation are also pronounced. For the southern hemisphere
463 savannah area, a slight increase in precipitation (approximately 10%, Fig. 3d) was simulated,
464 which is caused by strengthened convective activity (which coincides with enhanced
465 radiation and latent heat fluxes) in the rainy season (DJF, Fig. A4.). This can be considered as
466 a local effect of tree LAI increase. However, changes in precipitation are not restricted only
467 to the areas where tree cover increases (Fig. 3d, Fig. 4a), which is suggestive of remote
468 effects on tropical precipitation. This is further investigated in the sections below.

469 ***3.3 Vegetation feedback effects on circulation and precipitation***

470 Vegetation feedbacks on temperature in our simulations operate mainly via an increased
471 surface area for evaporation and a stronger coupling to the atmosphere as tree cover, root
472 depth and LAI increase relative to grasses, most notably in savannah areas, resulting in a
473 shift of the evaporative fraction (ratio of latent heat flux to turbulent heat fluxes) and an

474 increase in surface roughness length. Overall, the turbulent heat fluxes increase, which
475 tends to cool the surface and the lower atmosphere, exceeding the opposing (warming)
476 effects of increased vegetation cover on albedo, thus resulting in an overall cooling effect.
477 Similar behaviour was seen in southern Europe in a previous study with RCA-GUESS
478 (Wramneby et al., 2010).

479 The variability of precipitation over Africa is greatly influenced by the moisture advection
480 from the ocean to land. Previous studies have noted on the influence of Atlantic Walker
481 circulation on central African precipitation, as well as the role of the west African monsoon
482 for precipitation over western Africa (e.g. Nicholson and Grist, 2003;Dezfuli and Nicholson,
483 2013;Pokam et al., 2014). These circulation systems are associated with thermal contrasts
484 between ocean and land, creating a pressure contrast that tends to promote the movement
485 of moist surface air from the Atlantic over land. We examined the land-ocean thermal
486 contrast (∇T) and geopotential contrast ($\nabla\phi$) between the equatorial Atlantic and the near-
487 coast African continent for three pressure levels between 850 hPa and 975 hPa, to
488 characterise the circulation in the lower troposphere. We found that changes in ∇T and $\nabla\phi$
489 are highly inter-annually anti-correlated for the rainy seasons MAM and SON ($r=-0.82$ and -
490 0.64, respectively, Fig. 5; ~~Fig. A5~~Fig.). The sensitivity of $\nabla\phi$ to ∇T , depicted as the slope in Fig.
491 5, is generally maintained in the future, with a slight decrease in the sensitivity for DJF and a
492 slight increase for MAM.

493 Under the NFB future simulation, ocean-land contrast becomes larger (the absolute value of
494 ∇T increases by about 0.5-1°C, Table A2) as land temperature increases more than the GCM-
495 simulated increase in SSTs provided as forcing to the regional model (Fig. A3.). Differential
496 changes in features of the surface and lower atmosphere, such as changes in land-ocean

497 contrasts in boundary layer lapse rate (Joshi et al., 2008) and changes in Bowen ratio over
498 land (Sutton et al., 2007) explain such divergence in temperatures between ocean and land.
499 As a result, except for SON, $\nabla\phi$ is generally simulated to increase in the course of the
500 simulation (Fig. A5 Fig.), with the largest shift occurring in MAM ($11.96 \text{ m}^2 \text{ s}^{-2}$ by the end of
501 21st century, Table A2). For SON, ∇T increases but $\nabla\phi$ does not, suggesting that the trend of
502 $\nabla\phi$ under climate change is associated with the GCM-derived boundary conditions, despite
503 the strong regional coupling with ∇T in terms of variability (Fig. A5 Fig.).
504 In contrast, the increase in the ∇T is dampened considerably when incorporating interactive
505 vegetation. The resulting reduction in ∇T offsets $\nabla\phi$ uniformly and statistically significantly
506 for all seasons, generally counteracting the climate change effect on $\nabla\phi$ (Fig. 5, Table A2).

507 ***3.4 Effects on Walker circulation and low-latitude precipitation***

508 The low-level equatorial westerlies are important to the central African rainfall. They are
509 associated with the lower branch of the Walker cell located near the western equatorial
510 coast of Africa, and they transfer moisture from the adjacent Atlantic to the eastern
511 equatorial coast and the Congo basin (e.g. Nicholson and Grist, 2003; Schefuß et al.,
512 2005; Cook and Vizy, 2015). These westerlies occur from March to October, being best
513 developed in JJA. They shift northward with the excursion of the Inter Tropical Convergence
514 Zone (ITCZ) and under the strong influence of the South Atlantic high pressure cell
515 (Nicholson and Grist, 2003). This pattern is simulated by RCA-GUESS for the present-day
516 climate (Fig. 6). Via this circulation system, moisture can reach far over the African landmass
517 at around 28°E , upwell and integrate into the mid-level African Easterly Jet (AEJ) (Camberlin
518 et al., 2001; Nicholson and Grist, 2003). RCA-GUESS reproduces this pattern with a realistic

519 magnitude (Fig. 6, Fig. 7, Fig. 8, Fig. 9) when compared with previous studies based on
520 reanalysis data (Camberlin et al., 2001; Nicholson and Grist, 2003).

521 In the NFB future simulation, equatorial westerlies are strengthened throughout the year
522 both over ocean (Fig. 6) and over land (Fig. 7). Changes in wind speed (Δu) can be explained
523 by changes in the low-level pressure contrast between land and ocean (sect. 3.3), where
524 strengthened $\nabla\phi$ leads to enhanced u , especially for MAM when the zonal pressure contrast
525 prevails (Table A2). Atmospheric specific humidity in the lower troposphere near the equator
526 also increases by around 10%-20% for MAM and SON, extending from the ocean to inland
527 along the equator (Fig. 8cd; Fig. 9cd). Meanwhile, changes in future rainfall are apparent
528 along the equator, with increases over the equatorial coastal or inland areas (Fig. A4.),
529 concurrent with stronger moisture inflow to land in the low-level troposphere (Fig. 8cd; Fig.
530 9cd).

531 Vegetation feedbacks are simulated to weaken the climate change enhancement of the
532 Walker circulation, resulting in a weakening of the equatorial westerlies and counteracting
533 the effects of climate change alone (Fig. 6i-l and Fig. 7i-l; Fig. 8ef and Fig. 9ef). These changes
534 correspond well to changes in low-level ocean-land geopotential contrast $\Delta\nabla\phi$ with the
535 biggest impact for MAM and SON (Table A2). The weakened Walker circulation is also
536 represented as suppressed vertical uplifting motions over central Africa (Fig. 8f and Fig. 9f).
537 Atmospheric specific humidity at 850 hPa is reduced by approximately 7% due to vegetation
538 feedbacks which are comparable to the contribution of climate change (Fig. 8ef vs. Fig. 8cd;
539 Fig. 9ef vs. Fig. 9cd).

540 Analysis of the moisture flux convergence also confirms the impacts of a weakened Walker
541 circulation (Fig. 10) on the hydrological cycle caused by vegetation feedback. Moisture fluxes
542 for most parts of the African continent diverge toward the ocean near the equatorial
543 regions. This divergence is similar for both MAM and SON but the effect is slightly stronger
544 for SON, which also corresponds to reduced humidity for these areas (Fig. 8e-f; Fig. 9e-f).

545 The changes in precipitation show a distinct spatial and temporal pattern with changes in
546 the rainbelt area (defined as 2mm day^{-1} contour with 10-days smoothing, Fig. 11). Under
547 future conditions, the rainbelt, which follows the ITCZ excursion, shifts around 3° northward
548 during JAS (Fig. 11a). As a result, rainfall intensity increases from May to October, with the
549 most pronounced increase by more than 30% relative to present-day levels of around 2 mm
550 day^{-1} on the margins of the rainbelt. The rainy season becomes longer for Sahel (+9 days) as
551 well as for central Africa (+1 day). The location of the rainbelt for the rest of the year
552 remains unchanged, but there is a pronounced increase in rainfall intensity for the southern
553 African rainy season (about 10%) and a decrease (about -10%) for the central African rainy
554 seasons.

555 On top of the non-feedback climate change effect, vegetation feedbacks tend to cause a
556 slight contraction of the rainbelt around the equator, and they impose a primarily
557 counteractive effect on rainfall intensity compared to the climate change alone simulation
558 (NFB). For central Africa, the considerable decrease in rainfall intensity in the dry season
559 leads to a slight equatorward shrinking of the rainbelt (approximately 2°) and a shorter rainy
560 season (on average 10 days, represented as a 4-day postponed onset and a 6-day earlier
561 end). For southern Africa, strengthened convective precipitation results in a longer rainy
562 season by on average 6 days. There is no pronounced effect for the Sahel regions except for

563 some sparse changes over time and in some areas. To investigate the effects on ITCZ
564 location, we analysed the position of the intertropical front (ITF) with a meridional wind
565 criterion (Sultan and Janicot, 2003) by examining the location of maximum vertical uplifting
566 wind speed at 850 hPa over Sahel in July and over southern Africa in January. However, we
567 did not find pronounced effects for ITF (not shown) suggesting that changes in the rainbelt
568 location for central Africa are mainly caused by changes in precipitation intensity rather
569 than by changes in meridional circulation.

570 ***4. Discussion***

571 ***4.1 Related tenets of Regional Earth System Modelling***

572 We investigated the coupled dynamics of climate and vegetation over Africa under a future
573 climate change scenario, applying a regional-scale ESM that dynamically couples a dynamic
574 representation of vegetation structure, composition and distribution to a physical climate
575 model at a comparatively high grid resolution. Uniquely among existing studies of climate
576 dynamics for Africa, this enabled us to isolate the regional biophysical feedbacks, which are
577 usually not easy to disentangle in a global application in which the effects of changes in
578 carbon-cycle and large-scale circulation tend to compound the biophysical effects.

579 In comparison with global ESMs, the added value from the regional ESMs lies in the
580 enhanced resolution obtained in a regional setup as presented in this study, allowing for a
581 more detailed representation of local surface features such as topography, land use,
582 vegetation change, and consequently possible related feedbacks, and also enhancing the
583 model's ability to capture climatic variability and extreme climatic events (Giorgi,
584 1995; Rummukainen, 2010, 2016). Improvements in the representation of local processes
585 may be expected to result in improved larger scale features (e.g. sea level pressure,

586 circulation patterns) (Diffenbaugh et al., 2005;Feser, 2006). For example, Kjellström et al.
587 (2005) found that reduced bias in surface air temperature – largely determined by local
588 energy balance – resulted in a better representation of interannual variability of mean sea
589 level pressure and circulation patterns, and improved the simulation of precipitation.

590 **4.2 African vegetation patterns and change**

591 Vegetation dynamics are critically important in modulating the evolution of the 21st century
592 climate in our study. Land use and grazing (Sankaran et al., 2005;Bondeau et al.,
593 2007;Lindeskog et al., 2013), which were not included in our study, represent additional
594 potentially important drivers of land surface changes. The historical vegetation state is also
595 relevant for future simulations, due to legacy effects lasting decades or even centuries
596 (Moncrieff et al., 2014) and their influences on climate-vegetation equilibria (Claussen,
597 1998;Wang and Eltahir, 2000). While our model exhibited a degree of bias in simulated
598 vegetation under the present climate, the overall distribution of the major vegetation types
599 of the continent (forest, savannah and grassland) was broadly correct. Arguably, vegetation
600 type is a more important determinant of climate-vegetation equilibrium than structural
601 parameters of a given type, such as LAI (Claussen, 1994;Wang and Eltahir, 2000).

602 Previous experimental (Kgope et al., 2010) and modelling (Sitch et al., 2008;Moncrieff et al.,
603 2014) studies highlight the potential importance of physiological effects of atmospheric CO₂
604 concentrations on the productivity and water use efficiency of vegetation, particularly in low
605 latitude and water-limited ecosystem types. Shrub encroachment and woody thickening has
606 been observed in water-limited areas including Sahel in recent decades, coinciding with
607 rising CO₂ concentrations (e.g. Liu et al., 2015). In our results, the simulated vegetation
608 dynamics are consistent with these trends, presenting a trajectory of increased woody plant

609 dominance (not shown), and a similar future vegetation pattern (Fig. 4) as in previous
610 modelling studies (e.g., Sitch et al., 2008; Moncrieff et al., 2014). The vegetation changes
611 simulated by our model under future climate forcing, are large ~~relative~~ compared to the bias
612 noted in the representation of present-day vegetation state. This provides some confidence
613 that the simulated future vegetation is not critically dependent on these biases and, in turn,
614 that the emergent mechanisms of vegetation-climate interaction and their consequences
615 for circulation and precipitation trends suggested by our study are robust.

616 ***4.3 Vegetation feedbacks and land-ocean temperature contrasts***

617 The land-ocean contrast is an important driver of continental precipitation, as it determines
618 the transport of moisture from ocean to land (e.g. Giannini et al., 2003; Giannini et al.,
619 2005; Fasullo, 2010; Boer, 2011; Lambert et al., 2011). The positive trend in Sahel rainfall over
620 recent decades is a good example of linking moisture transport to land-ocean contrast,
621 where changes in SSTs over adjacent tropical oceans around Africa are key to the fragile
622 balance that defines the regional circulation system (Camberlin et al., 2001; Rowell,
623 2001; Giannini et al., 2003). Land-surface feedback is found to modify the interannual to
624 interdecadal climate variability in this region by vegetation-induced albedo or
625 evapotranspiration effects (Zeng et al., 1999; Wang et al., 2004). In our study, the SSTs were
626 prescribed from GCM-generated data, therefore the altered land-ocean thermal contrast
627 between simulations with and without feedback originated solely from the changes in land
628 surface temperature, in turn attributable to vegetation dynamics. Although this represents a
629 land-forced mechanism in contrast to an ocean-forced one inferred in other studies (e.g.
630 Giannini et al., 2003; Tokinaga et al., 2012), the mechanisms are similar. Wind speed and
631 land-ocean temperature contrast are reduced by approximately by 0.2 m s^{-1} and 0.2°C ,

632 respectively, when vegetation feedbacks are enabled in our study (Fig. 5 and Table A2);
633 these are comparable to the changes simulated in other studies for the Sahel
634 (approximately 0.2-0.5 m s⁻¹ per 0.2°C (Giannini et al., 2005)) and for the Pacific Oceans
635 (approximately 0.3 m s⁻¹ per 0.3°C (Tokinaga et al., 2012)). However, the relative importance
636 of such changes may differ for local climate systems: the lower branch of the Walker cell
637 over the eastern tropical Atlantic Ocean, which we have focused on in this study, may be in
638 a fragile balance and is more vulnerable to changes in thermal contrasts (equatorial
639 westerlies slowed down by approximately 0.2 m s⁻¹ from less than 2 m s⁻¹ of the present-day
640 wind speed in rainy seasons, Table A2) compared to the stronger monsoonal circulation for
641 Sahel and the Walker cell over the equatorial Pacific Ocean (> 5 m per second wind speed in
642 their peak months, Young, 1999). Our results indicate that even a small disturbance of the
643 eastern Tropical Atlantic circulation cell may produce profound impacts (larger relative
644 reduction in precipitation compared with the studies by Giannini et al. (2005) and Tokinaga
645 et al. (2012)).

646 Similar to the local effects over semiarid region identified in a previous vegetation-feedback
647 study focusing on an African sub-domain (Yu et al., 2015), in which vegetation feedback
648 increases local precipitation, our study in advance presents a remote effect induced by
649 vegetation feedback over the African wet tropics that may not be easy to capture in a
650 smaller simulation domain. A larger domain including sufficient adjacent ocean could
651 enhance land-ocean interaction through changes in regional circulation and allow regional
652 teleconnection features, e.g. the influences of the tropical Atlantic on rainfall in Guinea
653 Coast and central Africa (Camberlin et al., 2001; Nicholson and Grist, 2003), and link
654 between the Mediterranean Sea and Sahelian rainfall (Rayner et al., 2003), to develop.

655 | Despite biases in the present-day precipitation and vegetation state (LAI) for some regions,
656 | our model was able to reproduce the present-day land cover type, and the simulated
657 | present-day~~te~~ climate is close to previous study (Nikulin et al., 2012) using the same physical
658 | sub-model with observed land cover type. Under future climate change, vegetation-induced
659 | changes in circulation, thus a substantial change in moisture transport and precipitation, are
660 | mainly triggered by changes in land cover type (Fig. 4a), therefore, we argue that the
661 | influences from biases in initial conditions on such mechanism found in this study should be
662 | limited. Our study used prescribed SST forcing from a GCM and could thus not account for
663 | additional or opposing feedbacks mediated by ocean dynamics. However, as the ocean heat
664 | capacity is relatively large and variation in land-ocean thermal contrast can be greatly
665 | buffered by ocean heat uptake (Lambert and Chiang, 2007), we suggest that results should
666 | not change fundamentally if a dynamic ocean component was introduced to the model.

667 | ***5. Conclusion and outlook***

668 | We investigated the potential role of vegetation-mediated biophysical feedbacks on climate
669 | change projections for Africa in the 21st century. In current savannah regions, enhanced
670 | forest growth results in a strong evaporative cooling effect. We also identify alterations in
671 | the large-scale circulation induced by savannah vegetation change, resulting in remote
672 | effects and modulation of tropical rainfall patterns over Africa, favouring savannah
673 | ecosystems at the expense of equatorial rainforest. Our results point to the potential
674 | importance of vegetation-atmosphere interactions for regional climate dynamics and trends,
675 | and motivate the incorporation of vegetation dynamics and land-atmosphere biophysical
676 | coupling in regional models. This has become the standard in global climate modelling, but
677 | remains rare in regional climate modelling.

678 Future work can include detailed studies on the role of vegetation feedbacks in the regional
679 climate projections with respect to shorter-term dynamics such as climate variability and
680 extreme events, which may have crucial implications for landscape processes such as
681 wildfire. Regional and global biogeochemical feedbacks on future climate change may be
682 triggered by regional biophysical feedbacks, with implications for regional climatic trends,
683 variability and seasonality under future greenhouse forcing (Zhang et al., 2014). Impacts on
684 the carbon balance of semi-arid ecosystem like savannahs, known to respond sensitively to
685 variations in rainfall (Ahlström et al., 2015) may be particularly relevant to address for Africa.
686 The development of regional ESMs to account for the impacts of land use interventions such
687 as afforestation and reforestation, as well as forest clearing, grazing and fire management
688 may be a valuable next step, enabling land surface-atmosphere interaction studies linked to
689 socioeconomic scenarios and climate change mitigation strategies.

690

691

692

693

694

695

696

697

698 **Appendix A: Description of the coupling between RCA and LPJ-GUESS**

699 In RCA-GUESS, the LSS in RCA is coupled with LPJ-GUESS, which feeds back vegetation
700 properties to RCA. RCA provides net downward shortwave radiation, air temperature,
701 precipitation to LPJ-GUESS. In return, LPJ-GUESS provides daily updated LAI and the annually
702 updated tile sizes (determined from the simulated maximum growing season LAI summed
703 across tree and herbaceous PFTs in the previous year (Smith et al., 2011)). In the forest tile
704 in RCA, vegetation cover in this tile is estimated as the foliar projective cover (FPC) using
705 Beer's law:

706
$$A_{tree} = 1.0 - \exp(-0.5 \cdot LAI_{tree}), \quad (1)$$

707 where LAI_{tree} is the aggregated LAI of woody species, simulated by LPJ-GUESS in its forest
708 tile in which vegetation is assumed to comprise trees and understory herbaceous vegetation.

709 The natural vegetated fraction of the open land tile was calculated similarly:

711
$$A_{grass} = 1.0 - \exp(-0.5 \cdot LAI_{grass}), \quad (2)$$

712 where LAI_{grass} is the summed LAI of the simulated herbaceous PFTs from the herbaceous
713 tile of LPJ-GUESS in which only herbaceous vegetation is allowed to grow. The relative
714 covers of the forest and open land tiles affect surface albedo, which is a weighted average
715 of prescribed albedo constants for forest, open land and bare soil and controls the
716 absorption of surface incoming solar radiation, and therefore influences surface energy
717 balance and temperature.

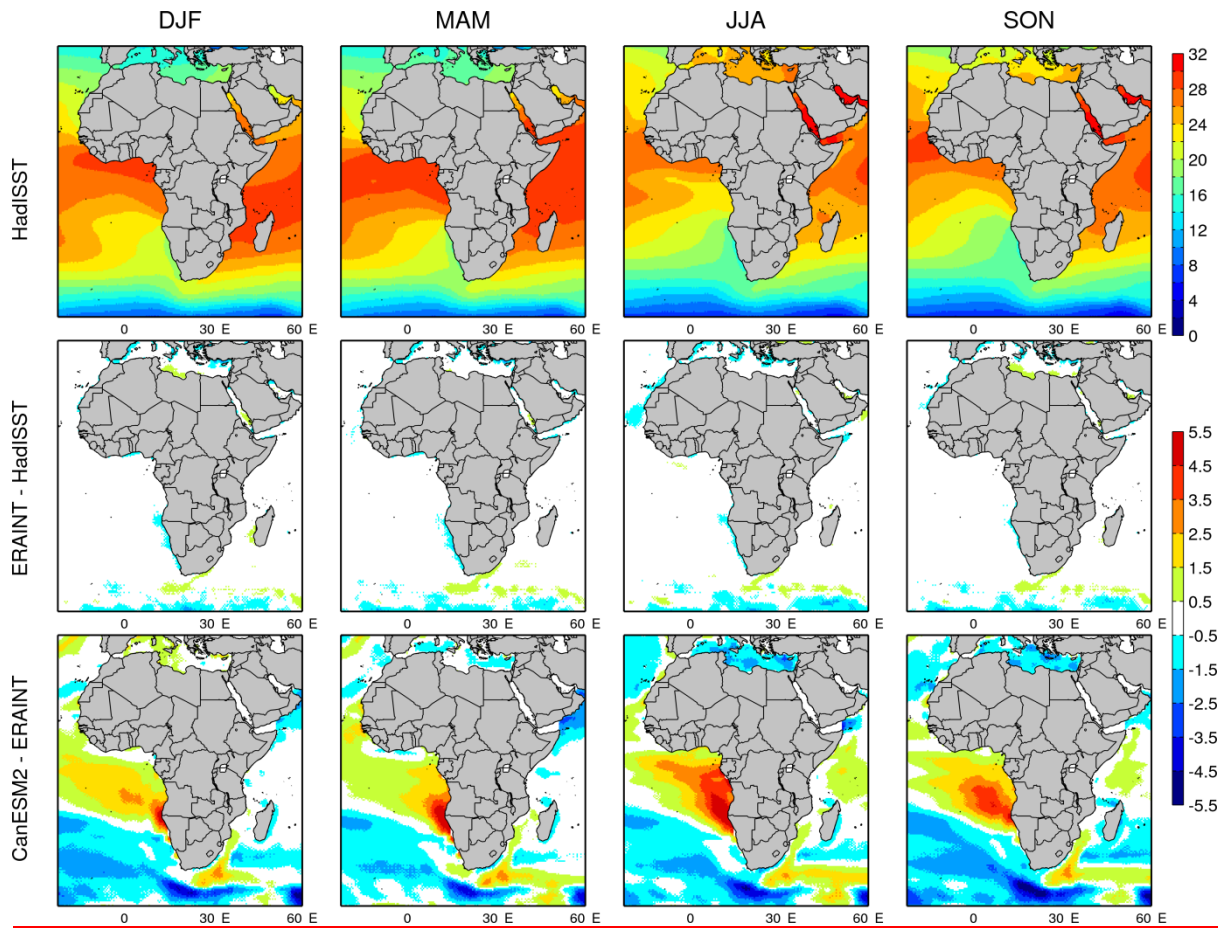
718
719 The turbulent heat fluxes are influenced by the properties of each tile, such as surface
720 roughness and surface resistance, which partly depend on vegetation properties provided
721 by LPJ-GUESS. The vegetation surface resistance controls vegetation transpiration and bare
722 soil evaporation for latent heat flux calculation. It scales with LAI and varies between the

723 different types of vegetation and affected by the incoming photosynthetically active
724 radiation, soil-water stress, vapour pressure deficit, air temperature and soil temperature.
725 The aerodynamic resistance controls both latent heat flux and sensible heat flux and is
726 influenced by surface roughness length distinguished from open land and forest. The total
727 heat fluxes and heat transfer determine the time evolution of the surface temperature and
728 thus the thermodynamics in the lower boundary layer. More details about the LSS are given
729 in Samuelsson et al. (2006), and the description of its coupling to the vegetation sub-model
730 is provided by Smith et al. (2011).

731 Table A1. Characteristics of the plant functional types (PFTs) used in the vegetation sub-model LPJ-GUESS.

Characteristics	NE	BE	TrBE	TrBR	TBS	IBS	C3G	C4G
Leaf phenology ^a	E	E	E	D	D	D	R	R
Drought tolerance	low	low	low	low	low	low	very low	very low
Shade tolerance	high	high	high	low	high	low	low	Low
Optimal temperature range for photosynthesis (°C)	10-25	15-35	25-30	25-30	15-25	10-25	10-30	20-45
Min T _c for survival (°C) ^b	-	1.7	15.5	15.5	-18	-	-	15.5

732 Notes: NE, needleleaved evergreen tree; BE, broadleaved evergreen tree; TrBE, tropical broadleaved
733 evergreen tree; TrBR, tropical broadleaved raingreen tree; TBS, shade-tolerant broadleaved summergreen tree;
734 IBS, shade-intolerant broadleaved summergreen tree; C3G, C3 grass or herb; C4G, C4 grass or herb;
735 ^aE, evergreen; D, deciduous; R, raingreen.
736 ^bT_c = mean temperature (°C) of coldest month of year.



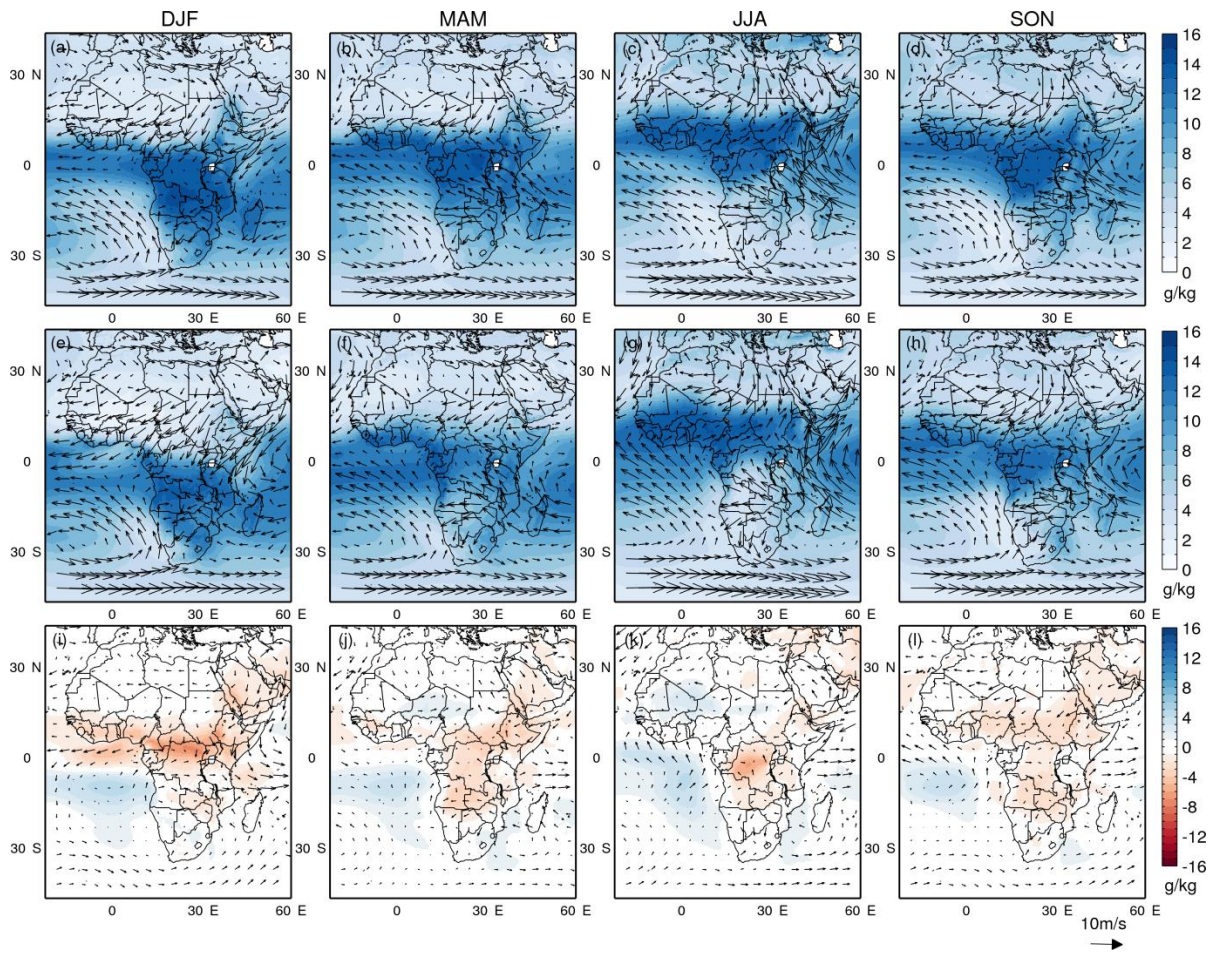
737

738

739

740

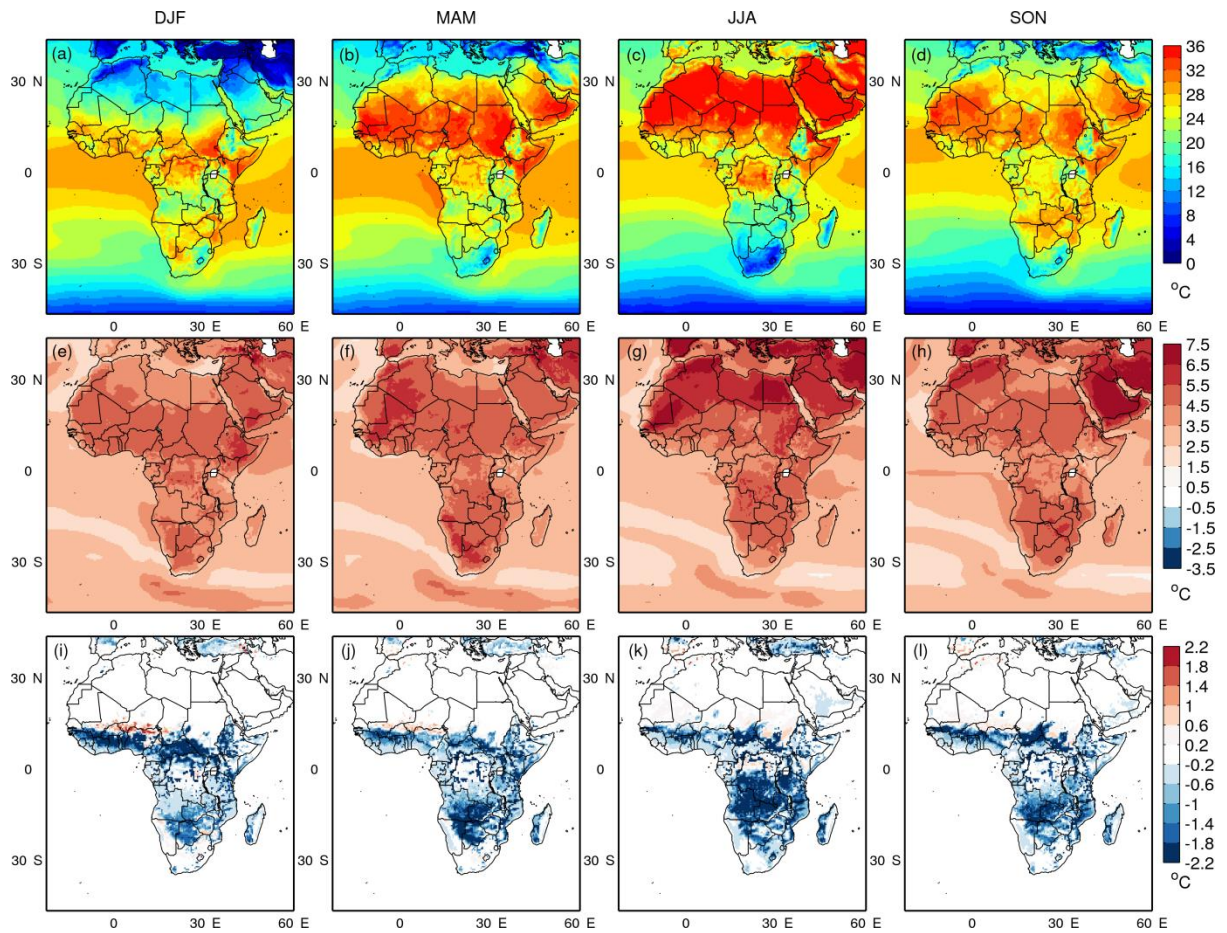
Fig. A1. Seasonal sea surface temperature ($^{\circ}\text{C}$) from the observational SST dataset HadISSTv1.1 (1st row, Rayner et al., 2003), and the biases of ERA-Interim (2nd row) and CanESM2 (3rd row) against the observed for the period 1997-2010.



741

742 | Fig. A2.1. Seasonal atmospheric circulation (arrows, m s^{-1}) and specific humidity (colour contours, g kg^{-1}) at
 743 | 850 hPa pressure level from ERA-Interim (1st row), NFB run (2nd row), as well as their differences (3rd row, NFB
 744 | minus ERA-Interim), for the period 1997-2010.

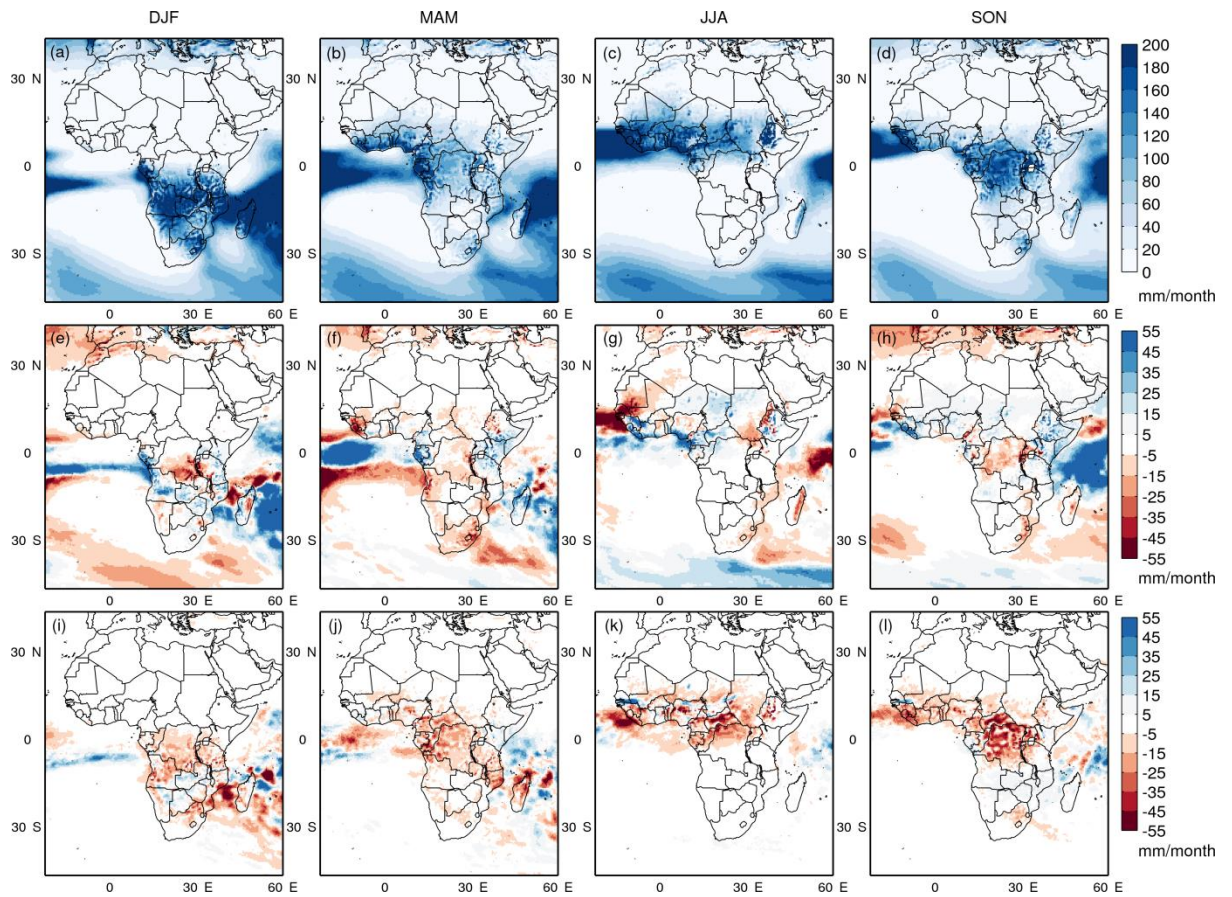
745



746

747 | Fig. A2A3. Simulated seasonal surface temperature for present day (a-d), for changes in future in the NFB
 748 experiment (e-h, future minus present day), and for changes from vegetation feedback in future (i-l, FB minus
 749 NFB for future). Definitions for calculation period, climate change signal and vegetation feedbacks are given in
 750 Sect. 2.2.

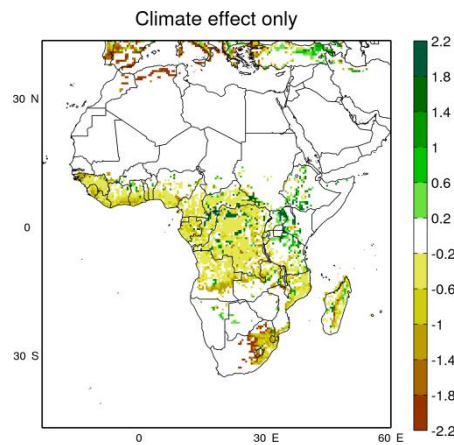
751



752

753

Fig. A3A4. Similar to Fig. A3., but for precipitation.



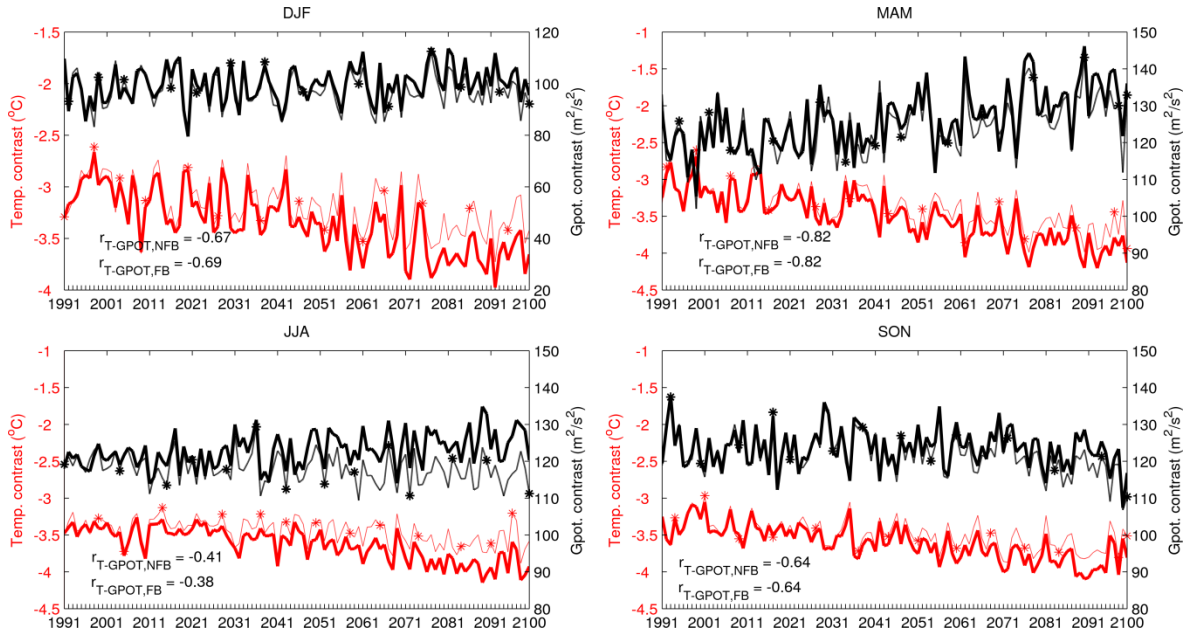
754

755

Fig. A4A5. Changes in forest tile LAI from the period 1991-2010 to the period 2081-2100 in FB_CC

756

experiment.



757

758 | Fig. A5A6. Annual changes in atmospheric ocean-land temperature contrast (∇T) and geopotential contrast
 759 ($\nabla \phi$) in time series for four seasons, represented by the mean contrast at the three pressure levels 850, 925
 760 and 975 hPa (ocean minus land) within the domain 15°N-15°S, 24°W-20°E (see the inset in the panel for JJA in
 761 Fig. 5). Correlation coefficient (r) between atmospheric temperature contrast (∇T) and geopotential contrast
 762 ($\nabla \phi$) are computed based on the de-trended annual time-series values for both FB (thick lines) and NFB (thin
 763 lines with asterisks) simulations. Changes between FB and NFB are significant at 95% confidence level for the
 764 whole time period. Note the different y-axis for DJF.

765 Table A2. Atmospheric temperature contrast, geopotential contrast and westerlies wind speed for the
 766 present-day state and contributions from climate change (CC subscript) and vegetation feedbacks (FB
 767 subscript), standard deviation is in parenthesis.

	DJF	MAM	JJA	SON
$\nabla T_{\text{present-day}} (^{\circ}\text{C})^a$	-3.06 (0.30)	-3.15 (0.34)	-3.47 (0.22)	-3.37 (0.24)
$\Delta \nabla T_{\text{CC}} (^{\circ}\text{C})^a$	-0.59*	-0.73*	-0.45*	-0.47*
$\Delta \nabla T_{\text{FB}} (^{\circ}\text{C})^a$	0.29*	0.23*	0.31*	0.22*
$\nabla \phi_{\text{present-day}} (\text{m}^2 \text{s}^{-2})^a$	98.14 (5.92)	120.86 (7.03)	120.94 (3.83)	124.08 (4.58)
$\Delta \nabla \phi_{\text{CC}} (\text{m}^2 \text{s}^{-2})^a$	3.94	11.96*	4.73*	-3.32
$\Delta \nabla \phi_{\text{FB}} (\text{m}^2 \text{s}^{-2})^a$	-4.93*	-3.86*	-8.96*	-3.92*
$U_{\text{zonal,present-day}} (\text{m s}^{-1})^b$	0.01 (0.27)	1.47 (0.32)	0.87 (0.37)	1.22 (0.31)
$\Delta U_{\text{zonal,CC}} (\text{m s}^{-1})^b$	0.35*	0.32*	0.68*	0.17*
$\Delta U_{\text{zonal,FB}} (\text{m s}^{-1})^b$	-0.00	-0.21*	-0.28*	-0.16*

768

Note: ^a: Calculations are same as Fig. 5.

769

^b: U_{zonal} is the averaged zonal wind speed for the pressure levels 850, 925 and 975 hPa between 3.5°N-6.5°N and 0-10°E; The positive represents westerly and the negative represents easterly.

770

*: Changes are significant at 95% confidence level using Mann-Whitney U-test (Hollander and Wolfe, 1999).

771

772

773

774 ***Acknowledgement***

775 This study is a contribution to the strategic research areas Modelling the Regional and
776 Global Earth System (MERGE) and Biodiversity and Ecosystem Services in a Changing Climate
777 (BECC). MCW would like to thank Paul Miller and Grigory Nikulin for their helpful discussions
778 and comments on this work. The model simulations were performed at the National
779 Supercomputer Centre (NSC) in Linköping, Sweden.

780

781

782

783

784

785

786

787

788

789

790

791

792 **Reference**

- 793 Ahlström, A., Raupach, M. R., Schurgers, G., Smith, B., Arneeth, A., Jung, M.,
794 Reichstein, M., Canadell, J. G., Friedlingstein, P., and Jain, A. K.: The
795 dominant role of semi-arid ecosystems in the trend and variability of the
796 land CO₂ sink, *Science*, 348, 895-899, 2015.
- 797 Alo, C. A., and Wang, G.: Role of dynamic vegetation in regional climate
798 predictions over western Africa, *Climate dynamics*, 35, 907-922, 2010.
- 799 Anav, A., Friedlingstein, P., Kidston, M., Bopp, L., Ciais, P., Cox, P., Jones, C.,
800 Jung, M., Myneni, R., and Zhu, Z.: Evaluating the Land and Ocean
801 Components of the Global Carbon Cycle in the CMIP5 Earth System Models,
802 *Journal of Climate*, 26, 6801-6843, 10.1175/jcli-d-12-00417.1, 2013.
- 803 Arora, V., Scinocca, J., Boer, G., Christian, J., Denman, K., Flato, G., Kharin, V.,
804 Lee, W., and Merryfield, W.: Carbon emission limits required to satisfy
805 future representative concentration pathways of greenhouse gases,
806 *Geophysical Research Letters*, 38, 2011.
- 807 Avissar, R., and Werth, D.: Global hydroclimatological teleconnections
808 resulting from tropical deforestation, *Journal of Hydrometeorology*, 6, 134-
809 145, 2005.
- 810 Berrisford, P., Dee, D., Fielding, K., Fuentes, M., Kallberg, P., Kobayashi, S.,
811 and Uppala, S.: The ERA-Interim Archive, 2009.
- 812 Boer, G.: The ratio of land to ocean temperature change under global
813 warming, *Climate dynamics*, 37, 2253-2270, 2011.
- 814 Bonan, G. B.: Forests and climate change: forcings, feedbacks, and the
815 climate benefits of forests, *science*, 320, 1444-1449, 2008.
- 816 Bondeau, A., Smith, P. C., Zaehle, S., Schaphoff, S., Lucht, W., Cramer, W.,
817 Gerten, D., LOTZE - CAMPEN, H., Müller, C., and Reichstein, M.: Modelling
818 the role of agriculture for the 20th century global terrestrial carbon balance,
819 *Global Change Biology*, 13, 679-706, 2007.
- 820 Brovkin, V., Claussen, M., Driesschaert, E., Fichefet, T., Kicklighter, D., Loutre,
821 M.-F., Matthews, H., Ramankutty, N., Schaeffer, M., and Sokolov, A.:
822 Biogeophysical effects of historical land cover changes simulated by six
823 Earth system models of intermediate complexity, *Climate Dynamics*, 26,
824 587-600, 2006.
- 825 Camberlin, P., Janicot, S., and Pocard, I.: Seasonality and atmospheric
826 dynamics of the teleconnection between African rainfall and tropical sea -
827 surface temperature: Atlantic vs. ENSO, *International Journal of*
828 *Climatology*, 21, 973-1005, 2001.
- 829 Charney, J. G.: Dynamics of deserts and drought in the Sahel, *Quarterly*
830 *Journal of the Royal Meteorological Society*, 101, 193-202, 1975.

831 Claussen, M.: On coupling global biome models with climate models,
832 *Climate Research*, 4, 203-221, 1994.

833 Claussen, M.: Modeling bio-geophysical feedback in the African and Indian
834 monsoon region, *Climate Dynamics*, 13, 247-257, 1997.

835 Claussen, M.: On multiple solutions of the atmosphere – vegetation system
836 in present - day climate, *Global Change Biology*, 4, 549-559, 1998.

837 Claussen, M., and Gayler, V.: The greening of the Sahara during the mid-
838 Holocene: results of an interactive atmosphere-biome model, *Global*
839 *Ecology and Biogeography Letters*, 369-377, 1997.

840 Cook, K. H., and Vizy, E. K.: The Congo Basin Walker circulation: dynamics
841 and connections to precipitation, *Climate Dynamics*, 1-21, 2015.

842 Dezfuli, A. K., and Nicholson, S. E.: The relationship of rainfall variability in
843 western equatorial Africa to the tropical oceans and atmospheric
844 circulation. Part II: The boreal autumn, *Journal of Climate*, 26, 66-84, 2013.

845 Diffenbaugh, N. S., Pal, J. S., Trapp, R. J., and Giorgi, F.: Fine-scale processes
846 regulate the response of extreme events to global climate change,
847 *Proceedings of the National Academy of Sciences of the United States of*
848 *America*, 102, 15774-15778, 10.1073/pnas.0506042102, 2005.

849 Döscher, R., Wyser, K., Meier, H. M., Qian, M., and Redler, R.: Quantifying
850 Arctic contributions to climate predictability in a regional coupled ocean-
851 ice-atmosphere model, *Climate Dynamics*, 34, 1157-1176, 2010.

852 Eklundh, L., and Olsson, L.: Vegetation index trends for the African Sahel
853 1982–1999, *Geophysical Research Letters*, 30, 2003.

854 Eltahir, E. A.: Role of vegetation in sustaining large-scale atmospheric
855 circulations in the tropics, *JOURNAL OF GEOPHYSICAL RESEARCH-ALL*
856 *SERIES-*, 101, 4255-4268, 1996.

857 Fasullo, J. T.: Robust Land-Ocean Contrasts in Energy and Water Cycle
858 Feedbacks*, *Journal of Climate*, 23, 4677-4693, 2010.

859 Feser, F.: Enhanced detectability of added value in limited-area model
860 results separated into different spatial scales, *Monthly weather review*, 134,
861 2180-2190, 2006.

862 Giannini, A., Saravanan, R., and Chang, P.: Oceanic forcing of Sahel rainfall
863 on interannual to interdecadal time scales, *Science*, 302, 1027-1030, 2003.

864 Giannini, A., Saravanan, R., and Chang, P.: Dynamics of the boreal summer
865 African monsoon in the NSIPP1 atmospheric model, *Climate Dynamics*, 25,
866 517-535, 2005.

867 Giorgi, F.: Perspectives for regional earth system modeling, *Global and*
868 *Planetary Change*, 10, 23-42, 1995.

869 Giorgi, F., Jones, C., and Asrar, G. R.: Addressing climate information needs
870 at the regional level: the CORDEX framework, *World Meteorological*
871 *Organization (WMO) Bulletin*, 58, 175, 2009.

872 Harris, I., Jones, P. D., Osborn, T. J., and Lister, D. H.: Updated high-
873 resolution grids of monthly climatic observations – the CRU TS3.10 Dataset,
874 *International Journal of Climatology*, 34, 623-642, 10.1002/joc.3711, 2014.

875 Herrmann, S. M., Anyamba, A., and Tucker, C. J.: Recent trends in vegetation
876 dynamics in the African Sahel and their relationship to climate, *Global*
877 *Environmental Change*, 15, 394-404,
878 <http://dx.doi.org/10.1016/j.gloenvcha.2005.08.004>, 2005.

879 Hickler, T., Eklundh, L., Seaquist, J. W., Smith, B., Ardö, J., Olsson, L., Sykes, M.
880 T., and Sjöström, M.: Precipitation controls Sahel greening trend,
881 *Geophysical Research Letters*, 32, 2005.

882 Hickler, T., Smith, B., Prentice, I. C., Mjofors, K., Miller, P., Arneth, A., and
883 Sykes, M. T.: CO₂ fertilization in temperate FACE experiments not
884 representative of boreal and tropical forests, *Global Change Biology*, 14,
885 1531-1542, 10.1111/j.1365-2486.2008.01598.x, 2008.

886 Hickler, T., Vohland, K., Feehan, J., Miller, P. A., Smith, B., Costa, L., Giesecke,
887 T., Fronzek, S., Carter, T. R., and Cramer, W.: Projecting the future
888 distribution of European potential natural vegetation zones with a
889 generalized, tree species - based dynamic vegetation model, *Global Ecology*
890 *and Biogeography*, 21, 50-63, 2012.

891 Hollander, M., and Wolfe, D. A.: in: *Nonparametric Statistical Methods*, 2nd
892 ed., John Wiley & Sons, New York 35-140, 1999.

893 Huffman, G. J., Adler, R. F., Morrissey, M. M., Bolvin, D. T., Curtis, S., Joyce, R.,
894 McGavock, B., and Susskind, J.: Global precipitation at one-degree daily
895 resolution from multisatellite observations, *Journal of Hydrometeorology*,
896 2, 36-50, 2001.

897 Jamali, S., Seaquist, J., Eklundh, L., and Ardö, J.: Automated mapping of
898 vegetation trends with polynomials using NDVI imagery over the Sahel,
899 *Remote Sensing of Environment*, 141, 79-89,
900 <http://dx.doi.org/10.1016/j.rse.2013.10.019>, 2014.

901 Jones, C., Giorgi, F., and Asrar, G.: The Coordinated Regional Downscaling
902 Experiment: CORDEX—an international downscaling link to CMIP5, *Clivar*
903 *Exchanges*, 16, 34-40, 2011.

904 Joshi, M. M., Gregory, J. M., Webb, M. J., Sexton, D. M., and Johns, T. C.:
905 Mechanisms for the land/sea warming contrast exhibited by simulations of
906 climate change, *Climate Dynamics*, 30, 455-465, 2008.

907 Keenan, T. F., Hollinger, D. Y., Bohrer, G., Dragoni, D., Munger, J. W., Schmid,
908 H. P., and Richardson, A. D.: Increase in forest water-use efficiency as
909 atmospheric carbon dioxide concentrations rise, *Nature*, 499, 324-327,
910 2013.

911 Kgope, B. S., Bond, W. J., and Midgley, G. F.: Growth responses of African
912 savanna trees implicate atmospheric [CO₂] as a driver of past and current
913 changes in savanna tree cover, *Austral Ecology*, 35, 451-463, 2010.

914 Kjellström, E., Bärring, L., Gollvik, S., Hansson, U., Jones, C., Samuelsson, P.,
915 Rummukainen, M., Ullerstig, A., Willén, U., and Wyser, K.: A 140-year
916 simulation of European climate with the new version of the Rossby Centre
917 regional atmospheric climate model (RCA3), 2005.

918 Kjellström, E., Nikulin, G., Hansson, U., Strandberg, G., and Ullerstig, A.: 21st
919 century changes in the European climate: uncertainties derived from an
920 ensemble of regional climate model simulations, *Tellus A*, 63, 24-40, 2011.

921 Kucharski, F., Zeng, N., and Kalnay, E.: A further assessment of vegetation
922 feedback on decadal Sahel rainfall variability, *Climate dynamics*, 40, 1453-
923 1466, 2013.

924 Lambert, F. H., and Chiang, J. C.: Control of land - ocean temperature
925 contrast by ocean heat uptake, *Geophysical research letters*, 34, 2007.

926 Lambert, F. H., Webb, M. J., and Joshi, M. M.: The relationship between land-
927 ocean surface temperature contrast and radiative forcing, *Journal of*
928 *Climate*, 24, 3239-3256, 2011.

929 LaRow, T. E., Stefanova, L., and Seitz, C.: Dynamical simulations of north
930 Atlantic tropical cyclone activity using observed low-frequency SST
931 oscillation imposed on CMIP5 Model RCP4. 5 SST projections, *Journal of*
932 *Climate*, 27, 8055-8069, 2014.

933 Lawrence, D., and Vandecar, K.: Effects of tropical deforestation on climate
934 and agriculture, *Nature Climate Change*, 5, 27-36, 2015.

935 Lindeskog, M., Arneeth, A., Bondeau, A., Waha, K., Seaquist, J., Olin, S., and
936 Smith, B.: Implications of accounting for land use in simulations of
937 ecosystem carbon cycling in Africa, *Earth System Dynamics*, 4, 385-407,
938 2013.

939 Liu, Y. Y., van Dijk, A. I. J. M., de Jeu, R. A. M., Canadell, J. G., McCabe, M. F.,
940 Evans, J. P., and Wang, G.: Recent reversal in loss of global terrestrial
941 biomass, *Nature Clim. Change*, 5, 470-474, 10.1038/nclimate2581

942 [http://www.nature.com/nclimate/journal/v5/n5/abs/nclimate2581.html](http://www.nature.com/nclimate/journal/v5/n5/abs/nclimate2581.html#supplementary-information)
943 [#supplementary-information](http://www.nature.com/nclimate/journal/v5/n5/abs/nclimate2581.html#supplementary-information), 2015.

944 Long, S.: Modification of the response of photosynthetic productivity to
945 rising temperature by atmospheric CO₂ concentrations: has its importance
946 been underestimated?, *Plant, Cell & Environment*, 14, 729-739, 1991.

947 Moncrieff, G. R., Scheiter, S., Bond, W. J., and Higgins, S. I.: Increasing
948 atmospheric CO₂ overrides the historical legacy of multiple stable biome
949 states in Africa, *New Phytologist*, 201, 908-915, 2014.

950 Morales, P., Hickler, T., Rowell, D. P., Smith, B., and Sykes, M. T.: Changes in
951 European ecosystem productivity and carbon balance driven by regional
952 climate model output, *Global Change Biology*, 13, 108-122, 2007.

953 Moss, R. H., Edmonds, J. A., Hibbard, K. A., Manning, M. R., Rose, S. K., Van
954 Vuuren, D. P., Carter, T. R., Emori, S., Kainuma, M., and Kram, T.: The next

955 generation of scenarios for climate change research and assessment,
956 *Nature*, 463, 747-756, 2010.

957 Nicholson, S. E., and Grist, J. P.: The seasonal evolution of the atmospheric
958 circulation over West Africa and equatorial Africa, *Journal of Climate*, 16,
959 1013-1030, 2003.

960 Nikulin, G., Jones, C., Giorgi, F., Asrar, G., Büchner, M., Cerezo-Mota, R.,
961 Christensen, O. B., Déqué, M., Fernandez, J., Hänsler, A., van Meijgaard, E.,
962 Samuelsson, P., Sylla, M. B., and Sushama, L.: Precipitation Climatology in an
963 Ensemble of CORDEX-Africa Regional Climate Simulations, *Journal of*
964 *Climate*, 25, 6057-6078, 10.1175/JCLI-D-11-00375.1, 2012.

965 Nogherotto, R., Coppola, E., Giorgi, F., and Mariotti, L.: Impact of Congo
966 Basin deforestation on the African monsoon, *Atmospheric Science Letters*,
967 14, 45-51, 2013.

968 Olsson, L., Eklundh, L., and Ardö, J.: A recent greening of the Sahel—trends,
969 patterns and potential causes, *Journal of Arid Environments*, 63, 556-566,
970 2005.

971 Pokam, W. M., Bain, C. L., Chadwick, R. S., Graham, R., Sonwa, D. J., and
972 Kamga, F. M.: Identification of processes driving low-level westerlies in
973 West Equatorial Africa, *Journal of Climate*, 27, 4245-4262, 2014.

974 Rayner, N., Parker, D. E., Horton, E., Folland, C., Alexander, L., Rowell, D.,
975 Kent, E., and Kaplan, A.: Global analyses of sea surface temperature, sea ice,
976 and night marine air temperature since the late nineteenth century, *Journal*
977 *of Geophysical Research: Atmospheres*, 108, 2003.

978 Rowell, D. P.: Teleconnections between the tropical Pacific and the Sahel,
979 *Quarterly Journal of the Royal Meteorological Society*, 127, 1683-1706,
980 2001.

981 Rowell, D. P.: Simulating SST teleconnections to Africa: What is the state of
982 the art?, *Journal of Climate*, 26, 5397-5418, 2013.

983 Rummukainen, M.: State-of-the-art with regional climate models, *Wiley*
984 *Interdisciplinary Reviews: Climate Change*, 1, 82-96, 10.1002/wcc.8, 2010.

985 Rummukainen, M.: Added value in regional climate modeling, *Wiley*
986 *Interdisciplinary Reviews: Climate Change*, 7, 145-159, 10.1002/wcc.378,
987 2016.

988 Samuelsson, P., Gollvik, S., and Ullerstig, A.: The land-surface scheme of the
989 Rossby Centre regional atmospheric climate model (RCA3), SMHI, 2006.

990 Samuelsson, P., Jones, C. G., Willén, U., Ullerstig, A., Gollvik, S., Hansson, U.,
991 Jansson, C., Kjellström, E., Nikulin, G., and Wyser, K.: The Rossby Centre
992 Regional Climate model RCA3: model description and performance, *Tellus*
993 *A*, 63, 4-23, 2011.

994 Sankaran, M., Hanan, N. P., Scholes, R. J., Ratnam, J., Augustine, D. J., Cade, B.
995 S., Gignoux, J., Higgins, S. I., Le Roux, X., and Ludwig, F.: Determinants of
996 woody cover in African savannas, *Nature*, 438, 846-849, 2005.

997 Schefuß, E., Schouten, S., and Schneider, R. R.: Climatic controls on central
998 African hydrology during the past 20,000 years, *Nature*, 437, 1003-1006,
999 2005.

1000 Scheiter, S., and Higgins, S. I.: Impacts of climate change on the vegetation of
1001 Africa: an adaptive dynamic vegetation modelling approach, *Global Change*
1002 *Biology*, 15, 2224-2246, 2009.

1003 Sitch, S., Huntingford, C., Gedney, N., Levy, P. E., Lomas, M., Piao, S. L., Betts,
1004 R., Ciais, P., Cox, P., Friedlingstein, P., Jones, C. D., Prentice, I. C., and
1005 Woodward, F. I.: Evaluation of the terrestrial carbon cycle, future plant
1006 geography and climate-carbon cycle feedbacks using five Dynamic Global
1007 Vegetation Models (DGVMs), *Global Change Biology*, 14, 2015-2039,
1008 10.1111/j.1365-2486.2008.01626.x, 2008.

1009 Smith, B., Prentice, I. C., and Sykes, M. T.: Representation of vegetation
1010 dynamics in the modelling of terrestrial ecosystems: comparing two
1011 contrasting approaches within European climate space, *Global Ecology and*
1012 *Biogeography*, 10, 621-637, 10.1046/j.1466-822X.2001.t01-1-00256.x,
1013 2001.

1014 Smith, B., Samuelsson, P., Wramneby, A., and Rummukainen, M.: A model of
1015 the coupled dynamics of climate, vegetation and terrestrial ecosystem
1016 biogeochemistry for regional applications, *Tellus A*, 63, 87-106,
1017 10.1111/j.1600-0870.2010.00477.x, 2011.

1018 Smith, B., Warlind, D., Arneeth, A., Hickler, T., Leadley, P., Siltberg, J., and
1019 Zaehle, S.: Implications of incorporating N cycling and N limitations on
1020 primary production in an individual-based dynamic vegetation model,
1021 *Biogeosciences*, 11, 2027-2054, 2014.

1022 Sörensson, A. A., and Menéndez, C. G.: Summer soil–precipitation coupling
1023 in South America, *Tellus A*, 63, 56-68, 2011.

1024 Sultan, B., and Janicot, S.: The West African monsoon dynamics. Part II: The
1025 “preonset” and “onset” of the summer monsoon, *Journal of climate*, 16,
1026 3407-3427, 2003.

1027 Sutton, R. T., Dong, B., and Gregory, J. M.: Land/sea warming ratio in
1028 response to climate change: IPCC AR4 model results and comparison with
1029 observations, *Geophysical Research Letters*, 34, n/a-n/a,
1030 10.1029/2006GL028164, 2007.

1031 Sylla, M., Giorgi, F., Ruti, P., Calmanti, S., and Dell'Aquila, A.: The impact of
1032 deep convection on the West African summer monsoon climate: a regional
1033 climate model sensitivity study, *Quarterly Journal of the Royal*
1034 *Meteorological Society*, 137, 1417-1430, 2011.

1035 Taylor, K. E., Stouffer, R. J., and Meehl, G. A.: An overview of CMIP5 and the
1036 experiment design, *Bulletin of the American Meteorological Society*, 93,
1037 485-498, 2012.

1038 Texier, D., De Noblet, N., Harrison, S., Haxeltine, A., Jolly, D., Jousaume, S.,
1039 Laarif, F., Prentice, I., and Tarasov, P.: Quantifying the role of biosphere-
1040 atmosphere feedbacks in climate change: coupled model simulations for
1041 6000 years BP and comparison with palaeodata for northern Eurasia and
1042 northern Africa, *Climate Dynamics*, 13, 865-881, 1997.

1043 Thonicke, K., Venevsky, S., Sitch, S., and Cramer, W.: The role of fire
1044 disturbance for global vegetation dynamics: coupling fire into a Dynamic
1045 Global Vegetation Model, *Global Ecology and Biogeography*, 10, 661-677,
1046 10.1046/j.1466-822X.2001.00175.x, 2001.

1047 Tokinaga, H., Xie, S.-P., Deser, C., Kosaka, Y., and Okumura, Y. M.: Slowdown
1048 of the Walker circulation driven by tropical Indo-Pacific warming, *Nature*,
1049 491, 439-443, 2012.

1050 Wang, G., and Alo, C. A.: Changes in precipitation seasonality in West Africa
1051 predicted by RegCM3 and the impact of dynamic vegetation feedback,
1052 *International Journal of Geophysics*, 2012, 2012.

1053 Wang, G., Eltahir, E., Foley, J., Pollard, D., and Levis, S.: Decadal variability of
1054 rainfall in the Sahel: results from the coupled GENESIS-IBIS atmosphere-
1055 biosphere model, *Climate Dynamics*, 22, 625-637, 2004.

1056 Wang, G., and Eltahir, E. A.: Biosphere—atmosphere interactions over West
1057 Africa. II: Multiple climate equilibria, *Quarterly Journal of the Royal
1058 Meteorological Society*, 126, 1261-1280, 2000.

1059 Wårlind, D., Smith, B., Hickler, T., and Arneth, A.: Nitrogen feedbacks
1060 increase future terrestrial ecosystem carbon uptake in an individual-based
1061 dynamic vegetation model, *Biogeosciences*, 11, 6131-6146, 10.5194/bg-11-
1062 6131-2014, 2014.

1063 Weber, U., Jung, M., Reichstein, M., Beer, C., Braakhekke, M., Lehsten, V.,
1064 Ghent, D., Kaduk, J., Viovy, N., and Ciais, P.: The interannual variability of
1065 Africa's ecosystem productivity: a multi-model analysis, *Biogeosciences*, 6,
1066 285-295, 2009.

1067 Wramneby, A., Smith, B., and Samuelsson, P.: Hot spots of vegetation-
1068 climate feedbacks under future greenhouse forcing in Europe, *J. Geophys.
1069 Res.*, 115, D21119, 10.1029/2010jd014307, 2010.

1070 Wu, M., Knorr, W., Thonicke, K., Schurgers, G., Camia, A., and Arneth, A.:
1071 Sensitivity of burned area in Europe to climate change, atmospheric CO₂
1072 levels and demography: A comparison of two fire - vegetation models,
1073 *Journal of Geophysical Research: Biogeosciences*, 10.1002/2015JG003036,
1074 2015.

1075 Xu, Z., Chang, P., Richter, I., and Tang, G.: Diagnosing southeast tropical
1076 Atlantic SST and ocean circulation biases in the CMIP5 ensemble, *Climate
1077 dynamics*, 43, 3123-3145, 2014.

1078 Young, I.: Seasonal variability of the global ocean wind and wave climate,
1079 *International Journal of Climatology*, 19, 931-950, 1999.

1080 Yu, M., Wang, G., and Pal, J. S.: Effects of vegetation feedback on future
1081 climate change over West Africa, *Climate Dynamics*, 1-20, 2015.

1082 Zeng, N., Neelin, J. D., Lau, K.-M., and Tucker, C. J.: Enhancement of
1083 interdecadal climate variability in the Sahel by vegetation interaction,
1084 *Science*, 286, 1537-1540, 1999.

1085 Zhang, W., Jansson, C., Miller, P., Smith, B., and Samuelsson, P.:
1086 Biogeophysical feedbacks enhance the Arctic terrestrial carbon sink in
1087 regional Earth system dynamics, *Biogeosciences*, 11, 5503-5519, 2014.

1088 Zhou, L., Tian, Y., Myneni, R. B., Ciais, P., Saatchi, S., Liu, Y. Y., Piao, S., Chen,
1089 H., Vermote, E. F., Song, C., and Hwang, T.: Widespread decline of Congo
1090 rainforest greenness in the past decade, *Nature*, 509, 86-90,
1091 [10.1038/nature13265](https://doi.org/10.1038/nature13265), 2014.

1092 Zhu, Z., Bi, J., Pan, Y., Ganguly, S., Anav, A., Xu, L., Samanta, A., Piao, S.,
1093 Nemani, R. R., and Myneni, R. B.: Global data sets of vegetation leaf area
1094 index (LAI) 3g and Fraction of Photosynthetically Active Radiation (FPAR)
1095 3g derived from Global Inventory Modeling and Mapping Studies (GIMMS)
1096 Normalized Difference Vegetation Index (NDVI3g) for the period 1981 to
1097 2011, *Remote Sensing*, 5, 927-948, 2013.

1098

1099

1100

1101

1102

1103

1104

1105

1106

1107

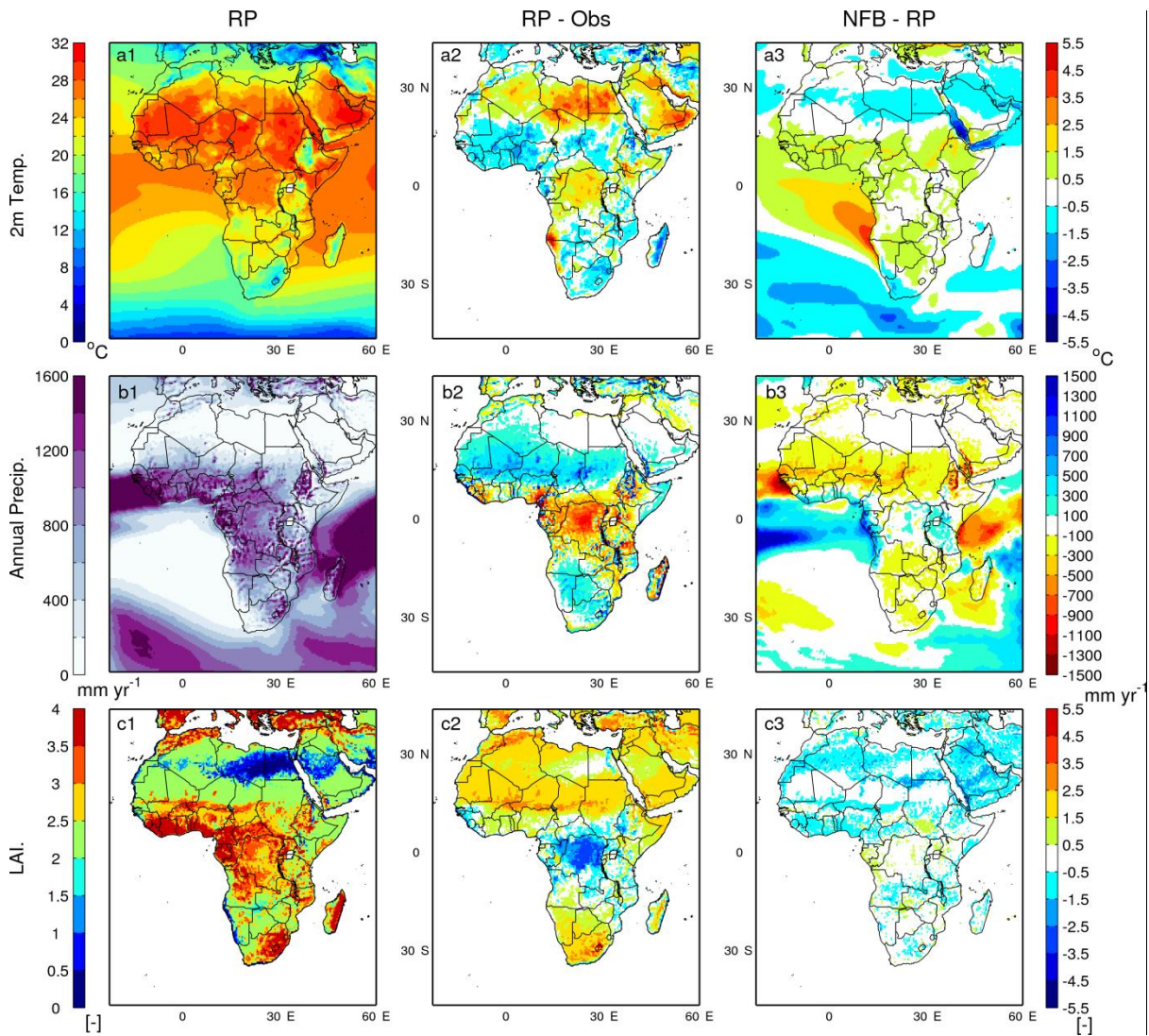
1108

1109

1110

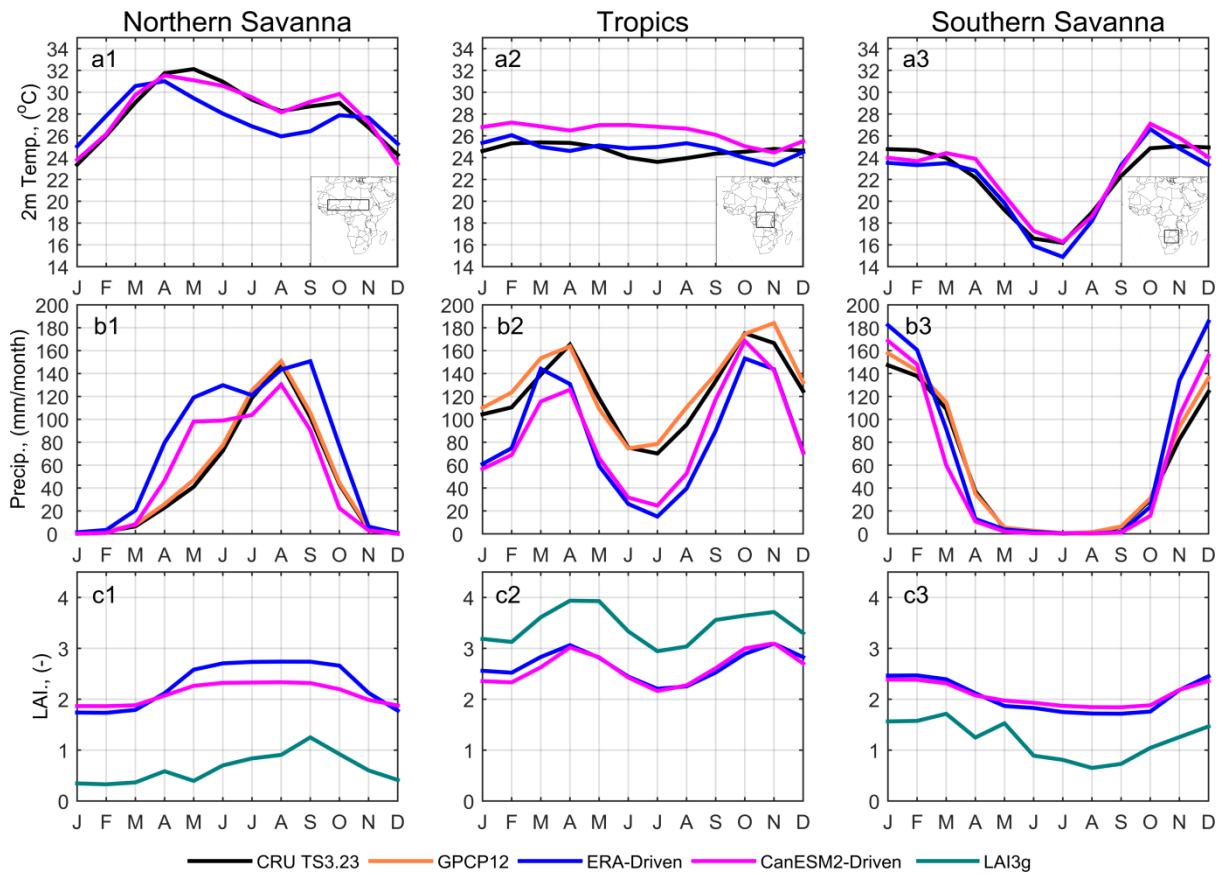
1111
1112

Figures and Tables



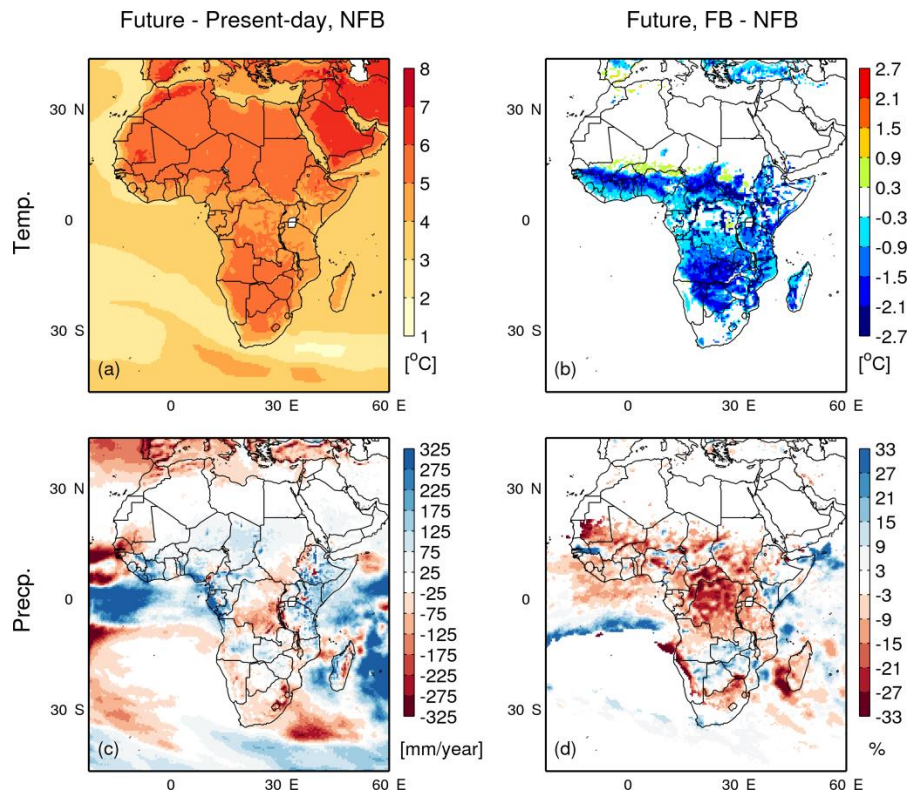
1113

1114 Fig. 1. Comparison between simulated and observed (a) annual mean near-surface air temperature, (b)
1115 annual precipitation and (c) annual maximum LAI for the period 1997-2010. Variables from the RP experiment
1116 (a1-c1) are compared with observations (a2-c2) and with those from the FB experiment (a3-c3), using RP
1117 minus observation and FB minus RP. For the comparison with observations (a2-c2), we used CRU temperature
1118 (a2) and precipitation (b2), as well as LAI3g (Zhu et al., 2013)(c2).



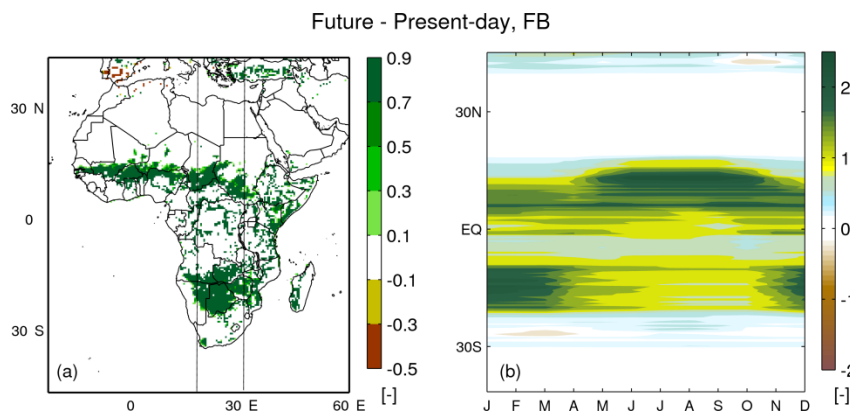
1120

1121 Fig. 2. Simulated seasonal cycle and observations for northern savannah (inset in a1), central Africa (inset
 1122 in a2) and southern savannah (inset in a3) for the period 1997-2010. 2m temperature (a1-a3) and precipitation
 1123 (b1-b3) are as Fig. 1. For LAI (c1-c3) monthly mean tile-weighted simulated LAI over the averaging period are
 1124 used to compare with the observation.



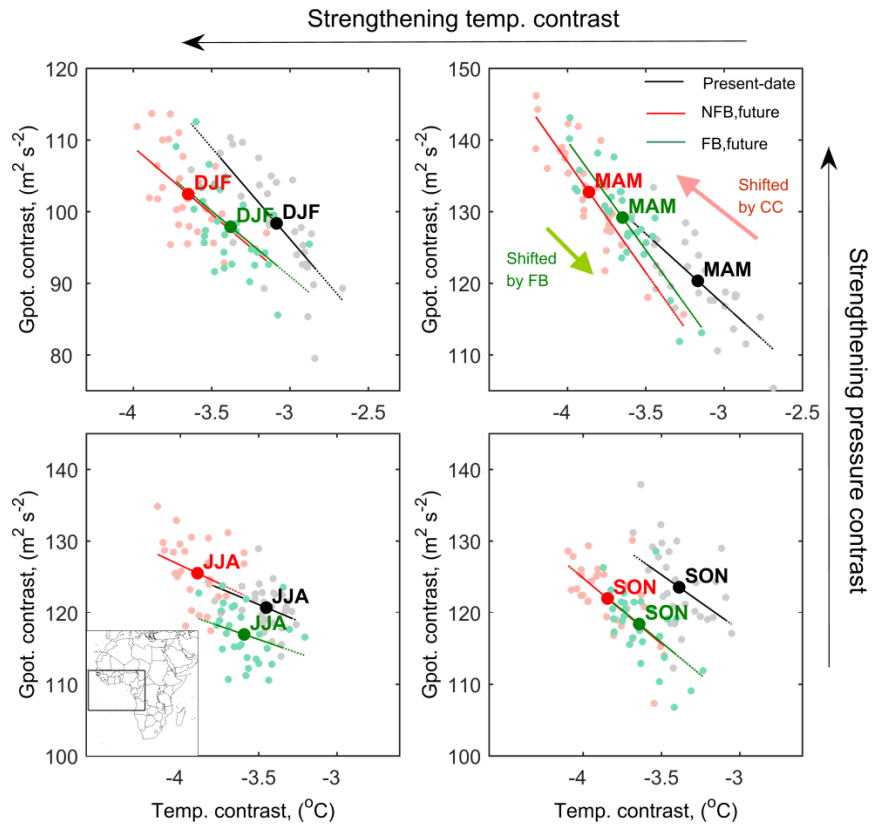
1125

1126 Fig. 3. Changes in surface temperature and precipitation due to climate change and vegetation feedback.
 1127 The calculation of climate change signal and vegetation feedbacks, present-day and future periods are defined
 1128 in Sect. 2.2. For (d), the percentage is calculated as the difference between FB and NFB (vegetation feedback)
 1129 divided by the present-day level and multiplied by 100. Grid points with annual mean precipitation <20 mm
 1130 year⁻¹ are skipped.



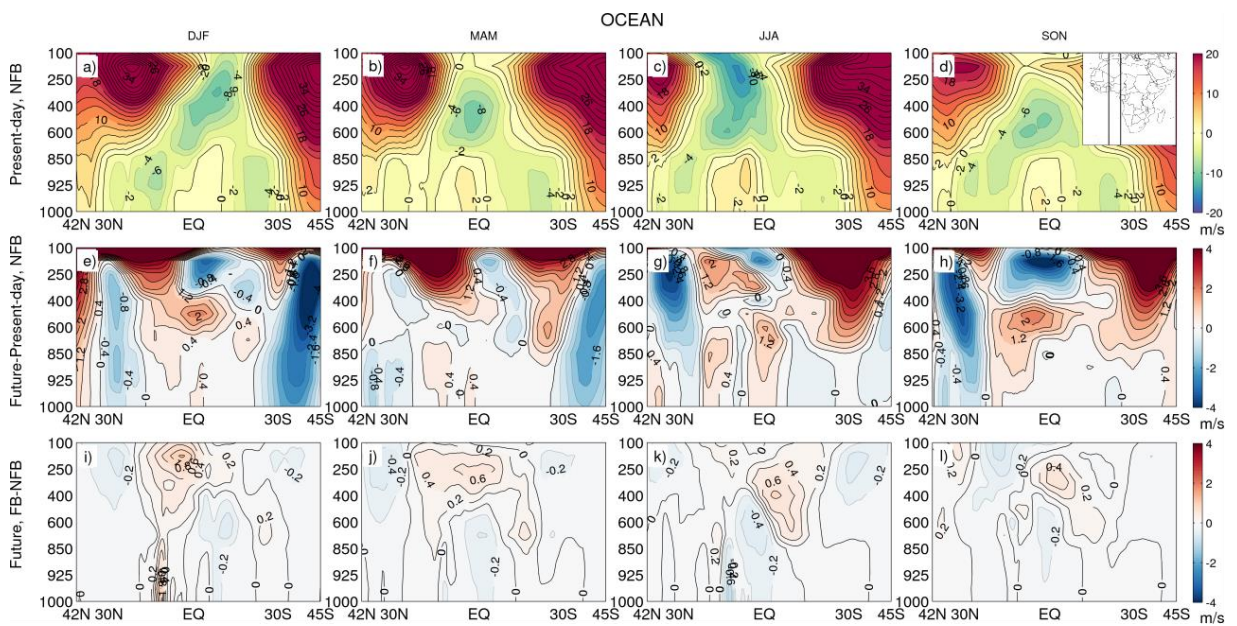
1131

1132 Fig. 4. (a) Change in forest fraction and (b) seasonal change in zonal mean forest LAI in the longitude band
 1133 between 18°E and 30°E (lines in a), calculated as future minus present-day in FB experiment. Present-day and
 1134 future periods are defined in Sect. 2.2.



1135

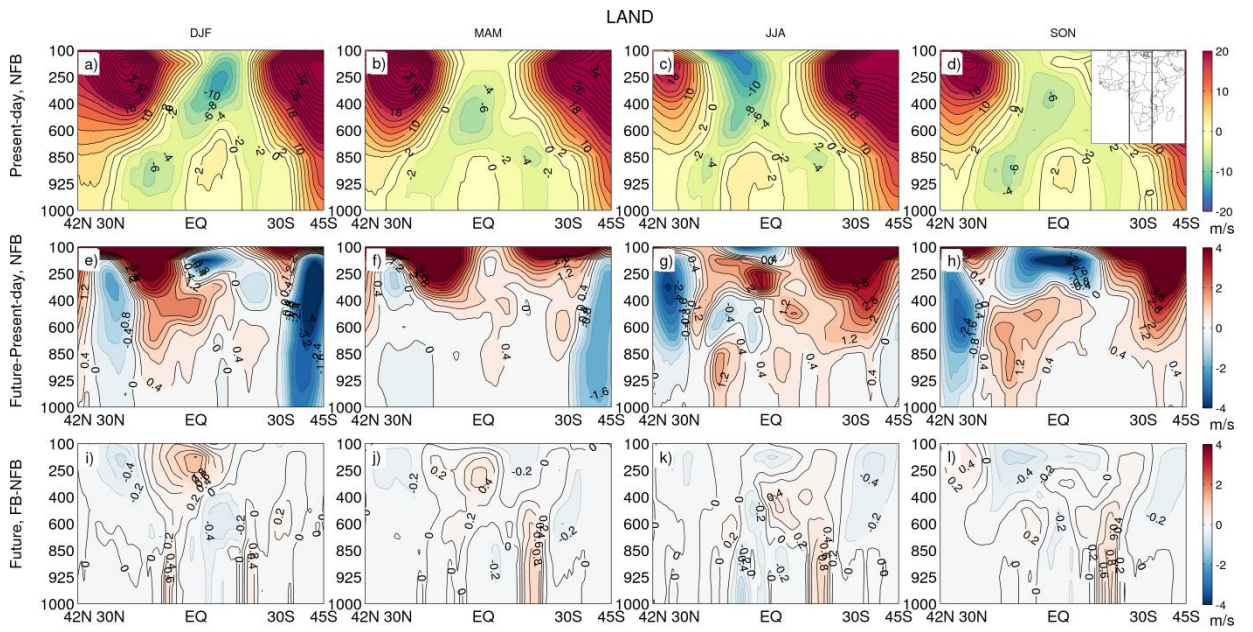
1136 Fig. 5. Changes in atmospheric ocean-land temperature contrast (∇T) and geopotential contrast ($\nabla\phi$),
 1137 represented by the mean contrast at the three pressure levels 850, 925 and 975 hPa (ocean minus land) within
 1138 the domain 15°N - 15°S , 24°W - 20°E (see the inset in the panel for JJA), for the NFB and FB simulation in the
 1139 present-day and the future period (as defined in Sect. 2.2). Each scatter point represents the relation between
 1140 $\nabla\phi$ and ∇T for the correspondent season of one year, and the slopes represent its sensitivity during the
 1141 selected periods.



1142

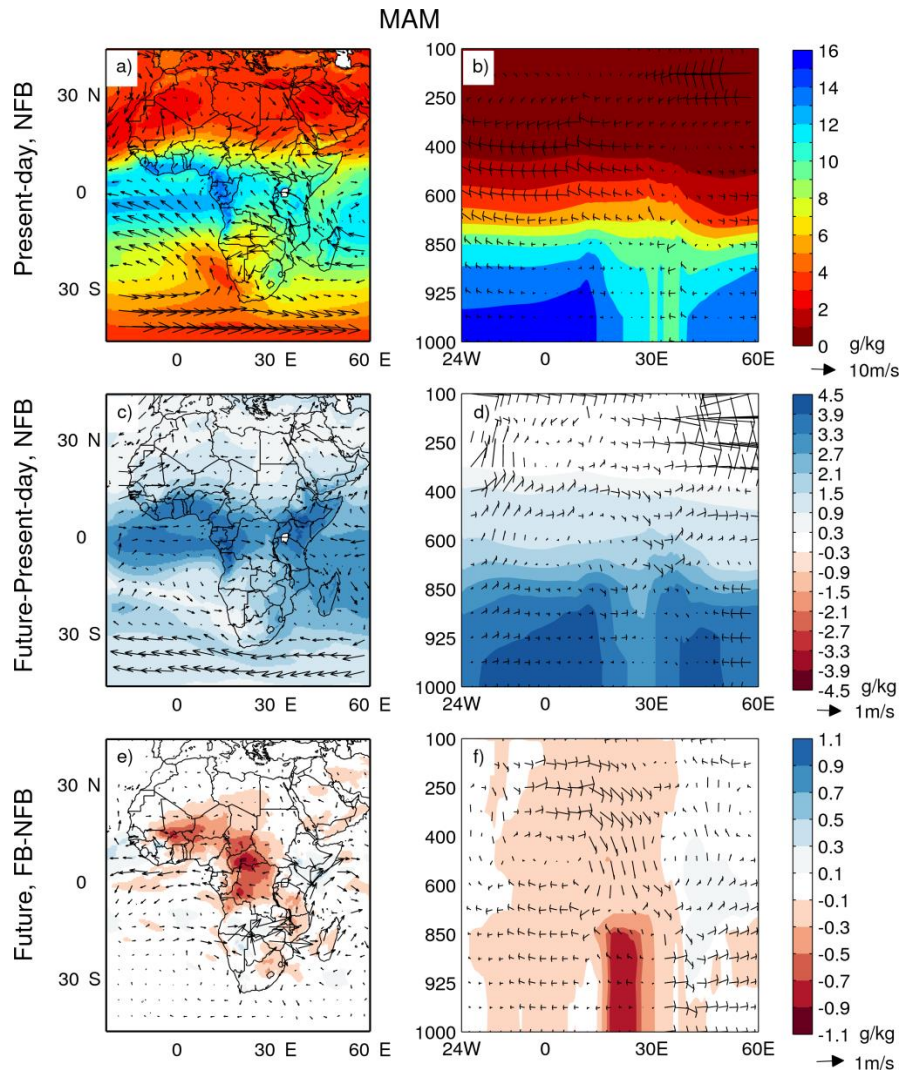
1143 Fig. 6. Seasonal mean zonal wind speed in a cross section over adjacent Atlantic ocean (0 - 10°E , see the
 1144 inset in d), for present-day (1st row), changes in future (future minus present-day, 2nd row) and the
 1145 differences between FB and NFB runs in future (FB minus NFB, 3rd row). Unit is m s^{-1} , positive values represent

1146 westerlies and negative values represent easterlies. Present-day and future periods are defined in Sect. 2.2
 1147 Contour intervals from top row to bottom row are 2m s^{-1} , 0.4m s^{-1} and 0.2m s^{-1} , respectively.



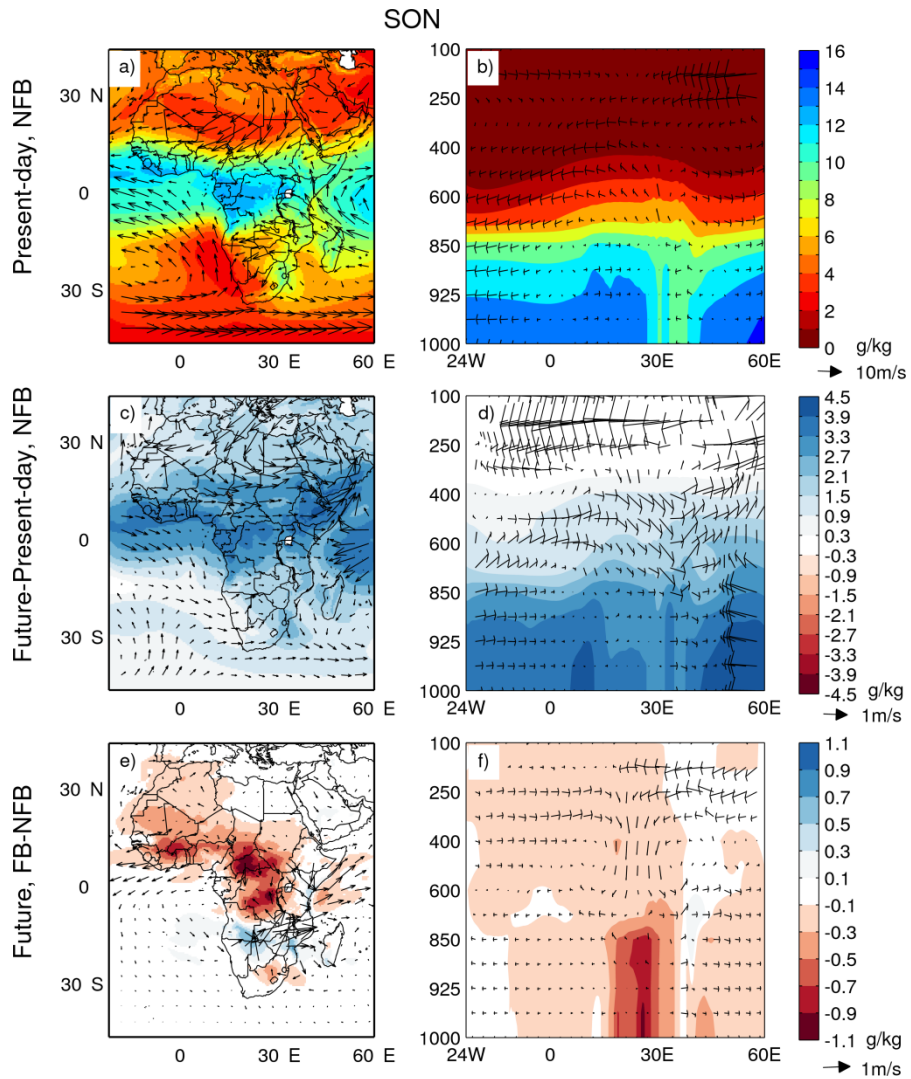
1148

1149 Fig. 7. As Fig. 6 but for longitudinal band over land ($10^{\circ}\text{E}-30^{\circ}\text{E}$, see the inset in d).



1150

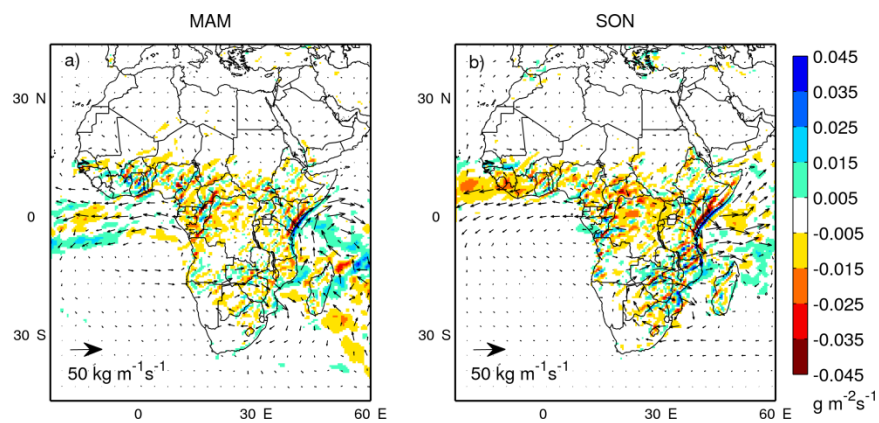
1151 Fig. 8. Atmospheric circulation (arrows, m s^{-1}) and specific humidity (colour contours, g kg^{-1}) at 850 hPa
 1152 pressure level for MAM, displayed as (a, c, e) for the entire domain, and (b, d, f) as a cross section for a latitude
 1153 band between 2.5°S and 2.5°N , for present day (top), climate change impacts (middle) and the vegetation
 1154 feedback (bottom). Definitions for calculation period, climate change signal and vegetation feedbacks are
 1155 given in Sect. 2.2.



1156

1157

Fig. 9. As Fig. 8 but for SON.



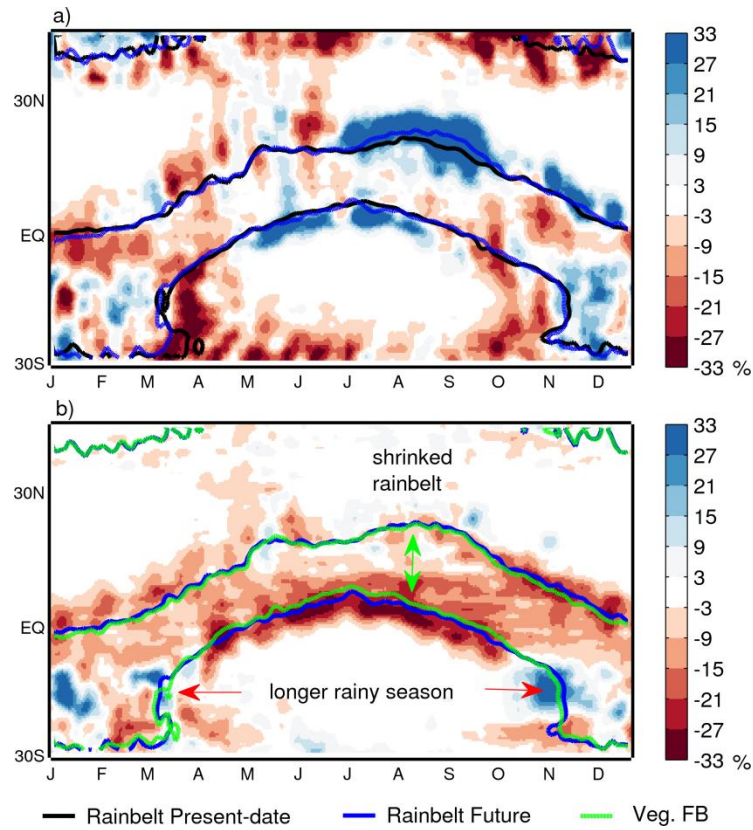
1158

1159

1160

1161

Fig. 10. Changes in vertically integrated moisture flux (arrows, $\text{kg m}^{-1} \text{s}^{-1}$) and moisture flux convergence (colour contours, $\text{g m}^{-2} \text{s}^{-1}$) caused by vegetation feedback, averaged over the future period (as defined in Sect. 2.2) for (a) MAM and (b) SON.



1162

1163 Fig. 11. Daily changes in precipitation averaged over the longitude band 18°E-30°E, represented as relative
 1164 changes in daily precipitation intensity (shading, %) and rainbelt location (contour) due to (a) climate change
 1165 and (b) vegetation feedback for future. The rainbelt location is defined as 2mm day⁻¹ contour. 10-day running
 1166 mean is applied for daily values.

1167 Table 1. Experimental design for the investigation of the vegetation-climate feedbacks in this study.

Runs	Vegetation Feedbacks	Radiative forcing ^a	CO ₂ forcing ^b for vegetation sub-model	Simulated period	Boundary condition
RP	Dynamic	Historical	Historical	1979-2011	ERA-Interim
FB	Dynamic	Transient under RCP8.5	Transient under RCP8.5	1961-2100	CanESM2
NFB	Prescribed vegetation simulated from 1961 to 1990	Transient under RCP8.5	Transient under RCP8.5	1991-2100	CanESM2
FB_CC	Dynamic	Transient under RCP8.5	Historical until 2005 and constant afterward	1991-2100	CanESM2

1168 Notes: a, using equivalent atmospheric CO₂ concentration; b, using actual atmospheric CO₂ concentration.

1169

1170

1171